

MAPPING THE GALACTIC HALO. I. THE “SPAGHETTI” SURVEY

HEATHER L. MORRISON¹

Department of Astronomy and Department of Physics, Case Western Reserve University, Cleveland, OH 44106-7215; heather@vegemite.cwru.edu

MARIO MATEO

Department of Astronomy, University of Michigan, 821 Dennison Building, Ann Arbor, MI 48109-1090; mateo@astro.lsa.umich.edu

EDWARD W. OLSZEWSKI AND PAUL HARDING

Steward Observatory, University of Arizona, 933 North Cherry Avenue, Tucson, AZ 85721; edo@as.arizona.edu, harding@billabong.astr.cwru.edu

R. C. DOHM-PALMER

Department of Astronomy, University of Michigan, 821 Dennison Building, Ann Arbor, MI 48109-1090; rdpalmer@astro.lsa.umich.edu

KENNETH C. FREEMAN AND JOHN E. NORRIS

Research School of Astronomy and Astrophysics, Mount Stromlo and Siding Spring Observatories, Australian National University, Private Bag, Weston Creek, ACT 2611, Canberra, Australia; kcf@mso.anu.edu.au, jen@mso.anu.edu.au

AND

MIWA MORITA

Steward Observatory, University of Arizona, 933 North Cherry Avenue, Tucson, AZ 85721; mmorita@as.arizona.edu

Received 1999 November 15; accepted 2000 January 27

ABSTRACT

We describe a major survey of the Milky Way halo designed to test for kinematic substructure caused by destruction of accreted satellites. We use the Washington photometric system to identify halo stars efficiently for spectroscopic follow-up. Tracers include halo giants (detectable out to more than 100 kpc), blue horizontal-branch (BHB) stars, halo stars near the main-sequence turnoff, and the “blue metal-poor stars” of Preston, Beers, & Shectman. We demonstrate the success of our survey by showing spectra of stars we have identified in all these categories, including giants as distant as 75 kpc. We discuss the problem of identifying the most distant halo giants. In particular, extremely metal-poor halo K dwarfs are present in approximately equal numbers to the distant giants for $V > 18$, and we show that our method will distinguish reliably between these two groups of metal-poor stars. We plan to survey 100 deg² at high Galactic latitude and expect to increase the numbers of known halo giants, BHB stars, and turnoff stars by more than an order of magnitude. In addition to the strong test that this large sample will provide for the question, Was the Milky Way halo accreted from satellite galaxies? we will improve the accuracy of mass measurements of the Milky Way beyond 50 kpc via the kinematics of the many distant giants and BHB stars we find. We show that one of our first data sets constrains the halo density law over Galactocentric radii of 5–20 kpc and z -heights of 2–15 kpc. The data support a flattened power-law halo with b/a of 0.6 and exponent -3.0 . More complex models with a varying axial ratio may be needed with a larger data set.

Key words: Galaxy: evolution — Galaxy: formation — Galaxy: halo — Galaxy: stellar content

1. INTRODUCTION

How much of the Galaxy’s halo was accreted from satellite galaxies? What fraction of these accretions has left substructure that we can detect today? Hierarchical galaxy formation pictures (Davis et al. 1985; Governato et al. 1997; Klypin et al. 1999) suggest that structure forms first in small clumps, which later combine to make larger galaxies. While this picture describes dark matter rather than stars, it is reasonable to expect that some stars would have formed in these dense clumps of matter at early times. This is borne out by the fact that almost all of the Local Group dwarf galaxies contain stars with ages greater than 10 Gyr (Mateo 1998). In studies of the Milky Way, the first suggestion that the Galaxy’s halo did not form in a fast, uniform collapse (Eggen, Lynden-Bell, & Sandage 1962) was made by Searle & Zinn (1978), who noted that the horizontal-branch (HB) morphology of the outer halo globular clusters could be explained by a younger mean age. These clusters would

have originated in “transient protogalactic fragments that continued to fall into dynamic equilibrium with the Galaxy for some time after the collapse of its central regions.”

Strong variations in the Galaxy’s potential associated with the formation of the inner disk and bar, plus the shorter orbital timescales there, may have erased the kinematic signature of halo accretion in its inner regions. Substructure may persist for many gigayears further from the Galactic center (Johnston, Spergel, & Hernquist 1995; Harding et al. 2000). We see evidence for accretion not only in the Sgr dwarf galaxy, which is being tidally disrupted on its current passage close to the Galaxy’s disk (Ibata, Gilmore, & Irwin 1994), but also in the detection of various moving groups in the halo field (Majewski, Munn, & Hawley 1994; Helmi et al. 1999). These latter objects are particularly interesting and surprising because they are at relatively small distances from the Galactic center (8–10 kpc).

Figure 1 (*top*) shows in histogram form the numbers of distant halo objects known to date. Globular clusters and dwarf spheroidal galaxies are not included. It is not surprising, with such small samples, that almost all the dis-

¹ Cottrell Scholar of Research Corporation and NSF CAREER Fellow.

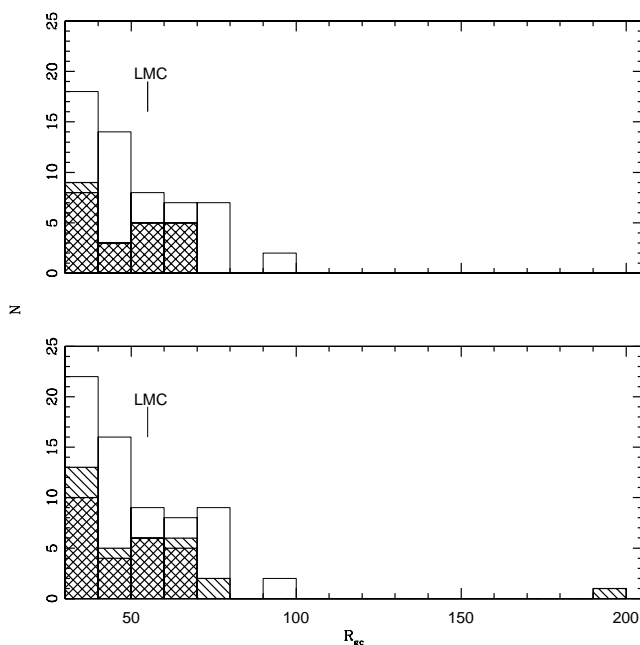


FIG. 1.—*Top*: Histogram of Galactocentric distances to halo field stars with $R_{gc} > 30$ kpc known to date. HB (RR Lyrae variables and BHB stars) stars are shown by cross-hatches, red giants are shown by hatches, and carbon stars comprise the rest. References for sources are given in Table 1. *Bottom*: Histogram of distances to outer halo field stars with the red giants and BHB stars of Olszewski et al. (2000) added—these stars were all confirmed spectroscopically during a single KPNO 4 m run. The giant at 190 kpc needs a confirming spectrum with higher S/N before we can be 100% confident of its luminosity.

coveries of halo substructure to date have been serendipitous. In this paper, we will describe a survey that will give a *quantitative* answer to the question, How much of the halo was accreted? by identifying a sample comprising a large number of halo stars out to great distances. (The bottom panel of Fig. 1 shows how the situation has improved after our first spectroscopic follow-up run on the Kitt Peak National Observatory [KPNO] 4 m telescope. References for sources in Fig. 1 are given in Table 1.)

In § 2, we discuss the design of our survey and the tracers we use, together with the region of the halo that each tracer will sample. Section 3 discusses our photometric selection technique in detail for each tracer, showing its efficacy with

spectra of stars found in each category. We also discuss the possible contaminants of our sample and how we reject them. Section 4 uses the numbers of turnoff stars found by our survey in various directions to constrain the density distribution of the halo. Future papers in this series will discuss our simulations of the breakup of satellites and their observational consequences (Harding et al. 2000), our photometric survey (Dohm-Palmer et al. 2000), and our spectroscopy of distant metal-poor giants and blue horizontal-branch (BHB) stars (Olszewski et al. 2000).

2. SURVEY DESIGN

Because substructure is visible in velocity space long after it disappears in density space (Johnston et al. 1995; Harding et al. 2000), we aim to obtain velocity data on a large sample of halo stars. Harding et al. (2000) discuss the signature that tidally disrupting streams will show in velocity histograms: although the observed signature does depend on the viewing geometry and initial conditions of the accretion, in many cases velocity histograms will be bimodal or multimodal. The features that correspond to disrupted satellites will show a velocity dispersion of order 10s of kilometers per second. Because substructure will survive longest in the outer Galaxy, distant halo tracers are advantageous. If we restrict our spectroscopic follow-up to 4 m-class telescopes, this means that halo red giants and BHB stars are the tracers of choice because of their intrinsic luminosity. However, these stars are intrinsically rare, and so they limit our detection methods for substructure—for example, it is impossible to find a sample of 100 halo giants in a field of size 1 deg^2 . Samples of this size are needed for methods of substructure detection based on velocity histograms. In order to have more sensitivity to subtle signatures of accretion, we also need tracers that are more numerous, such as halo turnoff stars. We shall, however, not be able to probe the extreme outer halo with these less luminous stars until 8 m-class telescopes are more generally available.

The stellar halo provides a very small fraction of the Milky Way's luminosity—in the solar neighborhood, the disk-to-halo star number ratio is $\sim 800:1$ (Bahcall & Casertano 1986; Morrison 1993), and even the thick disk outnumbers the halo by $\sim 40:1$. Thus it is important to use a method that will *efficiently* preselect halo stars before obtaining velocities.

2.1. Sky Coverage

When aiming to answer a question about the origin of the entire halo, all-sky coverage would be ideal. Johnston, Hernquist, & Bolte (1996) discuss such a survey for halo substructure, which, unfortunately, is not feasible at present. Existing all-sky surveys based on photographic plates cannot produce photometry accurate enough to efficiently select halo objects apart from rare BHB stars. Any spatial substructure in the halo will be washed out by the many foreground-disk and thick-disk stars in a photographic survey. The Sloan survey (Gunn 1995) plans to cover one-quarter of the sky at high Galactic latitude in the North. The photometry from this survey will be sufficiently accurate to enable the identification of halo turnoff stars and BHB stars, but not the rare distant red halo giants we discuss below. These stars, which will be inseparably contaminated by foreground K dwarfs in the Sloan colors, are

TABLE 1
LITERATURE SOURCES FOR FIGURE 1

Star Type	Reference
RR Lyrae	Hawkins 1984 Ciardullo, Jacoby, & Bond 1989 Suntzeff et al. 1991 Wetterer & McGraw 1996
BHB	Norris & Hawkins 1991 Flynn et al. 1995 Olszewski et al. 2000
Red giant	Ratnatunga & Freeman 1989 Croswell et al. 1991 Olszewski et al. 2000
Main sequence	Majewski 1992
Carbon	Totten & Irwin 1998

particularly valuable for this project because they probe the extreme outer halo.

We have chosen to use a pencil-beam survey of various high-latitude fields, using CCD photometry and the Washington system to select the halo stars, and we then carry out follow-up spectroscopy to search for kinematic substructure. Even with the most extreme hypothesis, that the entire halo is composed of tidal streams, their filling factor on the sky will still be small. Some fields will therefore contain more stars than the average and some considerably fewer. A large number of different pointings is preferable to maximize the chance of hitting a single stream. For example, assuming a typical dimension for a stream of $2^\circ \times 100^\circ$, 50 of these would cover only 25% of the sky. We have chosen to survey initially 100 deg^2 of the sky, in 100 different fields randomly distributed at high Galactic latitude (generally above $|b| = 45^\circ$), with most fields having Galactic longitude between 90° and 270° .

We chose in general to stay away from the quadrants that include the Galactic center for two reasons. First, structure is more readily destroyed close to the Galactic center, which lowers our chance of detecting it. The best place to look for substructure is the outer halo, where dynamical times are long and tidal forces small. Thus, the Galactic anticenter is better since the Galactocentric radii of the stars we detect will be larger. Second, there are many components represented at the Galactic center—young and old disk, thick disk, and bar, as well as the inner halo. Interpretation of our results would be more complex there because of the dynamical effect of the bar. The metal-weak tail of the thick disk is also minimized when we look at higher latitudes.

2.2. Tracers

Traditional ways of searching for halo stars include the following:

Proper-motion surveys (Sandage & Fouts 1987; Carney & Latham 1987; Ryan & Norris 1991). These surveys identify stars at most a few hundred parsecs away, except for the surveys of Majewski (1992) and Méndez et al. (1999), which produced complete proper-motion information on a sample of stars to $B = 22.5$ and 19, respectively (a maximum distance of 30 kpc).

RR Lyrae surveys (Kinman, Wirtanen, & Janes 1965; Saha 1985; Suntzeff, Kinman, & Kraft 1991; Wetterer & McGraw 1996; Kinman et al. 1996). These surveys sample more distant objects, but because of their extreme rarity—of order 1 per square degree—few distant RR Lyraes are known.

Objective prism surveys, generally for metal-poor giants or stars near the main-sequence turnoff (Bidelman & MacConnell 1973; Ratnatunga & Freeman 1989; Beers, Preston, & Shectman 1985; Morrison, Flynn, & Freeman 1990). Because of the relatively high resolution needed to identify these stars spectroscopically, these surveys are in general restricted to relatively bright magnitudes and therefore relatively nearby objects.

BHB star surveys. The BHB stars are identified either from their unusually blue color (Sommer-Larsen & Christensen 1985; Norris & Hawkins 1991) or by using objective prism spectra near the Ca K line (Pier 1982, 1984; Beers et al. 1985). BHB stars are almost as rare as RR Lyrae variables, and their identification is complicated by the presence of halo blue stragglers, which have the same broadband colors as BHB stars but higher gravity. As Norris &

Hawkins (1991) show, the blue straggler fraction may be as high as 50% for samples of faint blue stars.

Carbon stars. These are extremely rare stars (of order 1 per 200 deg^2 ; Totten & Irwin 1998) that are identified easily from objective-prism spectra. Totten & Irwin (1998) review the currently known halo carbon stars and their properties. Distances are more uncertain for these stars than for any other tracer we have discussed.

Halo tracers we chose to use are as follows:

Red giants. These are identified photometrically using a luminosity indicator based on the Mg *b*/MgH feature at 5170 Å plus a metallicity indicator based on line blanketing near 4000 Å , with spectroscopic confirmation.

Blue horizontal-branch stars. These are identified by their color plus a spectroscopic check of gravity.

Stars at the main-sequence turnoff. These are identifiable from their blue color—the most metal-poor globular clusters have turnoff colors of $B - V \simeq 0.38$, while the thick-disk turnoff is $B - V \simeq 0.5$, so stars with colors between these two values are most likely halo turnoff stars.

Blue metal-poor (BMP) stars (Preston, Beers, & Shectman 1994). These are halo field stars with colors bluer than $B - V = 0.38$, thought to be younger main-sequence stars. When found in globular clusters, such stars are typically referred to as blue stragglers and may have a different origin from the field analogs.

We will discuss these tracers and possible contaminants in our sample below. We reject another halo tracer, RR Lyrae variables, because of the large amount of telescope time needed to identify and phase these variable stars. Our technique reliably identifies both turnoff stars from the halo and the more distant halo giants and BHB stars. Because of their different luminosities, these objects probe different regions of the Galactic halo. Turnoff stars can only reach to Galactocentric distances of 15–20 kpc using 4 m-class telescopes for spectroscopic follow-up, while red giants and BHB stars will reach to distances of more than 100 kpc. However, because of both shorter evolutionary timescales for giants and the strong decrease in halo density with Galactocentric distance ($\rho \propto r^{-3}$ or $r^{-3.5}$; Zinn 1985; Saha 1985), there are far fewer halo giants detected than turnoff stars. Different techniques are therefore used to search for the kinematic signatures of accretion. For the more numerous turnoff stars, we use statistical techniques based on the appearance of the velocity histogram (testing for multimodality, for example, see Harding et al. 2000). For the rarer red giants, we use the technique of Lynden-Bell & Lynden-Bell (1995; see also Lynden-Bell 1999) to search for stars with similar energies and angular momenta, indicating a common origin.

3. SELECTION TECHNIQUE

Our initial survey was done using the Burrell and Curtis Schmidt Telescopes, which have CCD fields of order 1 deg^2 . The Burrell Schmidt is fitted with a back-illuminated SITE 2048×4096 CCD with 1.5 pixel^{-1} , while the Curtis Schmidt (often) has a 2048×2048 back-illuminated Tektronix CCD with 2.4 pixel^{-1} . Now that large mosaics are available, we have extended the survey using the Cerro Tololo Inter-American Observatory (CTIO) 4 m with the Big Throughput Camera (BTC; field of 0.25 deg^2) and the eight-CCD National Optical Astronomy Observatories mosaics. Our spectroscopic follow-up observations have been made using the Hydra multiobject fiber spectrograph

on the 3.5 m WIYN² Telescope and the Ritchey-Chrétien (RC) spectrograph on the KPNO 4 m telescope. Future observations with the Hydra spectrograph on the CTIO 4 m telescope and the Magellan Telescope are planned.

The Washington photometric system combines strong metallicity sensitivity for late-type giants with broad filter passbands, which contribute to observing efficiency. We use this system for our survey, as its filters can be used for selection of all the other tracers we need as well. We describe transformations between the Washington system and the *BVI* system in the Appendix.

In each survey field (of area approximately 1 deg²), we obtain photometry using a modified Washington (Canterna 1976; Geisler 1984) filter set (*C*, *M*, 51, and *i'* filters). The large pixel area on the Schmidt Telescopes leads to a high sky level in the *I* band. Thus we use the Sloan *i'* filter, whose passband avoids the worst of the bright sky lines in the *I* band, in place of the Washington *T*₂ or *I* filters. This *i'* filter transforms readily to the Washington system.

Typical exposure times using back-illuminated CCDs and the 24 inch (0.61 m) Schmidt telescopes are 6000 s in *C* and *M*, 8400 s in 51, and 4800 s in *i'*. On the CTIO 4 m with the BTC mosaic, exposure times were 100 s in *M*, 500 s in *C*, 120 s in *T*₂, and 250 s in 51. These give typical errors of 0.015 mag in each filter for a *V* = 19 star. Our photometry will be discussed in more detail by Dohm-Palmer et al. (2000).

We have used the data of Schlegel, Finkbeiner, & Davis (1998) to estimate the values of reddening in our fields, and dereddened the Washington colors according to the prescriptions of Canterna (1976) and Harris & Canterna (1979). The reddening values are small, so this did not have a strong effect on our results in any case.

Figure 2 shows a typical color-magnitude diagram (CMD) with the position of the halo and thick-disk turnoffs marked. Since each tracer requires a different selection technique, we will discuss them separately.

3.1. Halo Giants

This tracer is the most exciting since it allows us to probe the extreme outer halo. These stars have been little used in the past because they are greatly outnumbered by foreground K dwarfs, and it is difficult to distinguish K dwarfs from giants without accurate intermediate-band photometry or spectroscopy. However, their potential is enormous: a metal-poor star near the giant branch tip with $M_V = -2$ and $V = 19.5$ (easily observable at medium resolution on a 4 m-class telescope) has a distance of 200 kpc! The combination of large CCD fields with the Washington photometric system makes the detection of such objects feasible for the first time.

These distant halo giants are rare. Using the simple model of Morrison (1993), we find that there are of order 1–10 halo giants per square degree down to $V = 20$, using a range of assumptions about the halo density distribution. In § 4, we will show that out to Galactocentric distances of 20 kpc, the halo density law is well described by a flattened power law with exponent -3.0 and flattening $b/a = 0.6$. If this density law continues to larger distances, we would

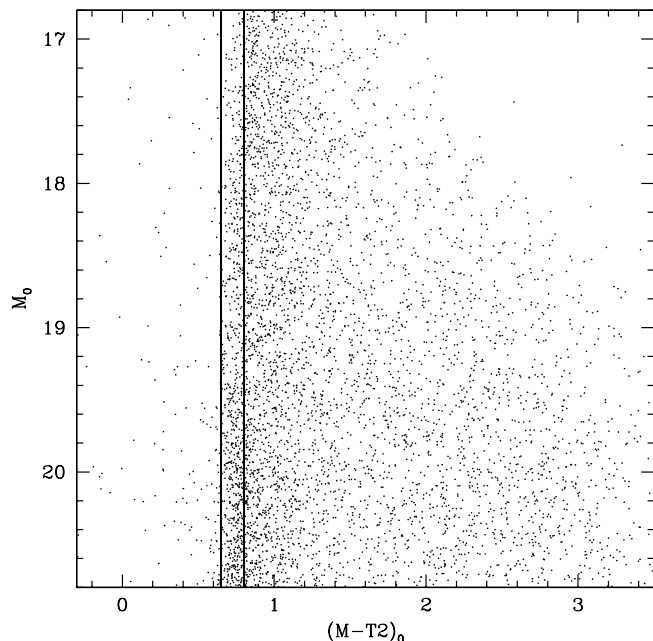


FIG. 2.—CMD ($M - T_2$ vs. M) for BTC fields of area 2.75 deg². Halo and thick-disk turnoffs are marked: the halo turnoff is the bluer one, at $(M - T_2)_0 = 0.64$.

expect to see four halo giants per square degree brighter than $V = 20$ at the north Galactic pole (NGP) and five per square degree in an anticenter field with Galactic latitude 45°.

There are three classes of objects found in the same range of color and magnitude as the halo giants we wish to find: (1) numerous K dwarfs of the thin and thick disk, which can be detected using a photometric survey ($M - 51$ color); (2) extremely metal-poor halo dwarfs, which are present in comparable numbers to halo giants for $V > 18$ and need a good follow-up spectrum (with signal-to-noise ratio $[S/N] \sim 15$) to distinguish from halo giants; and (3) background objects such as compact galaxies and quasi-stellar objects (QSOs), which are easily weeded out using a low-S/N follow-up spectrum.

3.1.1. Disk Dwarfs

The major source of contamination of a halo giant sample is foreground K dwarfs. To quantify the numbers of foreground dwarfs that we will need to weed out, we have estimated their number using a modified version of the Bahcall & Soniera (1984) model that includes both the thin and thick disks, using a 5% normalization for the thick disk. This predicts 70 thin-disk dwarfs and 90 thick-disk dwarfs ($0.9 < B - V < 1.2$) per square degree at the NGP.

Classical spectroscopic luminosity indicators (originally developed for Population I stars; see, e.g., Seitter 1970) are useful for our survey as follows:

1. The Mg *b* triplet and MgH band near 5200 Å are much stronger in dwarfs than giants in this color range. They begin to lose sensitivity to luminosity blueward of $B - V = 0.9$ ($M - T_2 = 1.2$). These features are also temperature sensitive.

2. The Ca I resonance line at 4227 Å shows marked sensitivity to both luminosity and temperature in K stars. Its strength increases as temperature and luminosity decrease. Since we have an independent photometric measure of tem-

² WIYN is a joint facility of the University of Wisconsin–Madison, Indiana University, Yale University, and the National Optical Astronomy Observatories.

perature from $M - T_2$ color, we can use the Ca I $\lambda 4227$ line as a luminosity indicator.

3. The blue and UV CN bands (band heads at 4216 and 3883 Å) are strong in giants and not in dwarfs. The bands become weaker with decreasing metallicity and are not visible below $[\text{Fe}/\text{H}] = -1.5$.

We have observed metal-poor dwarfs and giants in order to check whether these indicators retain their usefulness for more metal-poor stars. Our observations, plus those of the metal-weak giants we found, will be discussed in more detail by Olszewski et al. (2000). We use the Mg *b*/MgH region as our major method of rejecting disk dwarfs in our sample via photometric selection.

Geisler (1984) augmented the original Washington system with the David Dunlap Observatory (DDO) “51” filter, an intermediate-band filter centered on the Mg *b* and MgH features near 5200 Å, to give luminosity sensitivity for late G and K giants. The $M - 51$ color gives a photometric method of measuring the strength of these features. Figure 3 shows the strength of the MgH feature in spectra of dwarfs of solar and lower metallicity, and of the Mg *b* feature for giants of different metallicity. Most of these stars do not have direct measures of $M - T_2$ color. We transformed to Washington colors from existing $b - y$ or $B - V$ colors, using the method discussed in the Appendix. For ease of display we have sorted the stars into bins of metallicity and color. Table 2 gives sources of metallicity and color for all the stars shown in Figure 3.

These spectra clearly illustrate the luminosity indicators discussed above. A strong MgH band is seen for dwarfs with $M - T_2 = 1.2$. The feature becomes weaker as tem-

perature increases, until it is hard to see in the dwarfs with $M - T_2 = 1.0$. Although we do not have any spectra for dwarfs redder than $M - T_2 = 1.3$, the MgH band continues to strengthen with decreasing temperature. For all except the reddest giants ($M - T_2 > 1.45$), there is no MgH feature visible, and the Mg *b* lines are weak. For $M - T_2$ of 1.45 and redder, there is a slight MgH feature visible for the giants with $[\text{Fe}/\text{H}] = -1.0$ and above.

Our main method of detecting foreground dwarfs photometrically is via these features (MgH + Mg *b*). Other spectral features that are useful for luminosity discrimination with a follow-up spectrum are the Ca I $\lambda 4227$ line and the CN bands. The Ca I $\lambda 4227$ line is visible in all the dwarf spectra and can be seen to increase in strength as temperature decreases. It is also visible in the spectra of the metal-poor giants (especially above $[\text{Fe}/\text{H}] = -1.5$) but is much weaker than in dwarfs of the same color. Blue and UV CN bands are visible in the metal-rich giants (for example M71 stars I-1 and S232) and will be discussed in more detail in the next section.

The 51 filter gives us the ability to measure the strength of the MgH feature and reject the numerous foreground dwarfs. Precise photometry is necessary, however: Geisler (1984) obtained $M - 51$ colors for a sample of metal-rich and metal-poor giants and predominantly metal-rich dwarfs. He showed that giants and metal-rich dwarfs differ by at least 0.10 mag in $M - 51$ color for $B - V > 0.85$ and that the difference becomes more pronounced between metal-poor giants (with weaker Mg *b*) and metal-rich dwarfs.

Figure 4 shows $M - 51$ colors for known dwarf and giant stars. Geisler (1984) plotted $M - 51$ versus $T_1 - T_2$; it is clear

TABLE 2
LITERATURE SOURCES FOR METALLICITY AND COLOR FOR STARS IN FIGURE 3

Star ID	$[\text{Fe}/\text{H}]$	$b - y)_0$	$B - V)_0$	$V - I)_0$	$M - T_2)_0$	Reference
HD 98281	-0.25	0.46	0.97 ^a	Eggen 1998
HD 108564	-0.52	0.57	1.34 ^a	Eggen 1998
HD 134440	-1.52	0.973	1.22 ^b	Peterson 1981; Bessell 1990
HD 161848	-0.18	0.49	1.12 ^a	Eggen 1998
HD 165195	-2.1	0.73	1.53 ^a	Bond 1980
HD 182488	0.08	0.48	1.07 ^a	Eggen 1998
HD 190404	-0.44	1.114	Geisler 1984; Eggen 1998
BD + 52°1601	-1.8	0.55	1.18 ^a	Bond 1980
BD + 41°3306	-0.87	...	0.81	...	1.10 ^c	Peterson 1981; Carney 1979
BD + 09°2574	-2.4	0.54	1.17 ^a	Bond 1980; Twarog & Anthony-Twarog 1995
BD + 01°2916	-2.0	1.68	Bond 1980; Geisler 1986
BD - 00°4234	-0.99	0.58	1.36 ^a	Peterson 1981; Twarog & Anthony-Twarog 1995
G202-25	-0.38	...	0.87	...	1.15 ^c	Laird, Carney, & Latham 1988
NGC 5053 D	-2.58	...	1.01	...	1.3 ^c	Zinn 1985; Sandage, Katem, & Johnson 1977
M3 Cud 205	-1.66	...	1.36	...	1.75 ^c	Zinn 1985; Cudworth 1979
M3 Cud 250	-1.66	...	0.94	...	1.20 ^c	Zinn 1985; Cudworth 1979
M3 Cud 354	-1.66	...	0.82	...	1.10 ^c	Zinn 1985; Cudworth 1979
M3 Cud 1327	-1.66	...	0.74	...	1.0 ^c	Zinn 1985; Cudworth 1979
NGC 6171 16	-0.99	...	1.11	...	1.45 ^c	Zinn 1985; Sandage & Katem 1964
NGC 6171 20	-0.99	...	1.06	...	1.3 ^c	Zinn 1985; Sandage & Katem 1964
NGC 6171 62	-0.99	...	1.29	...	1.7 ^c	Zinn 1985; Sandage & Katem 1964
M71 A1	-0.58	...	1.30	...	1.7 ^c	Zinn 1985; Cudworth 1985
M71 L1	-0.58	...	0.99	...	1.3 ^c	Zinn 1985; Cudworth 1985
M71 S232	-0.58	...	1.18	...	1.5 ^c	Zinn 1985; Cudworth 1985
M2 2	-1.62	1.20	1.50	Zinn 1985; Armandroff & Da Costa 1991

^a Value of $M - T_2$ derived from $b - y$.

^b Value of $M - T_2$ derived from $V - I$.

^c Value of $M - T_2$ derived from $B - V$ and likely to be less accurate than those derived from $b - y$ or $V - I$.

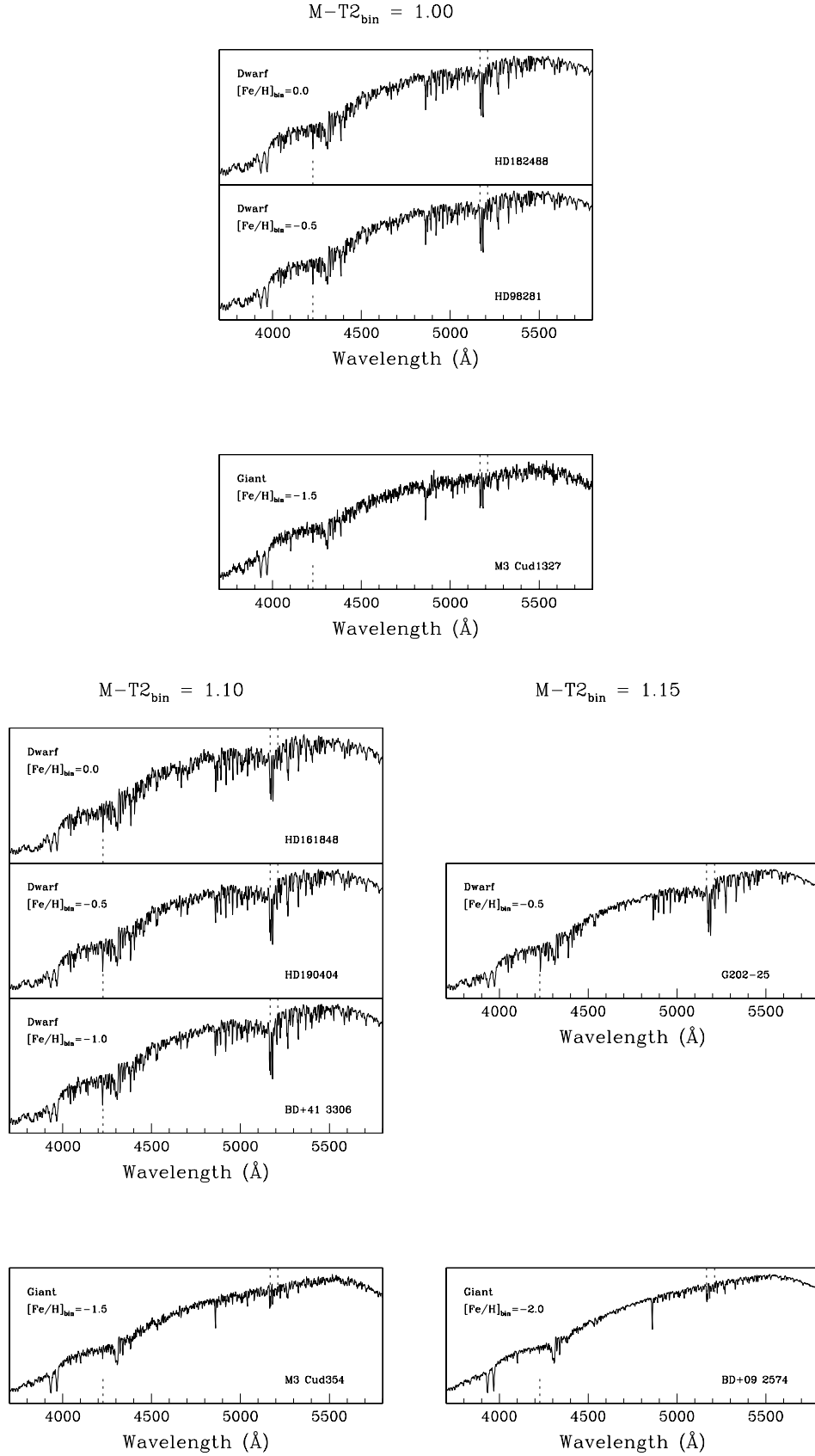
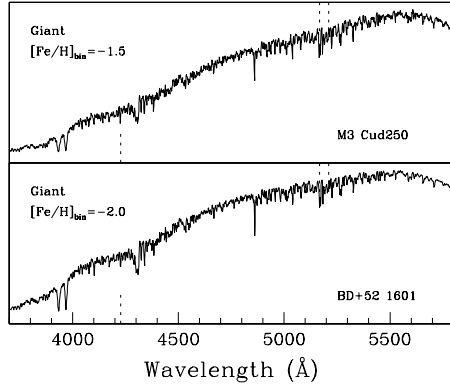
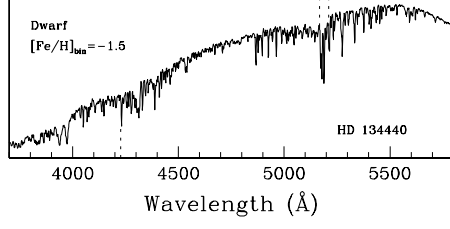
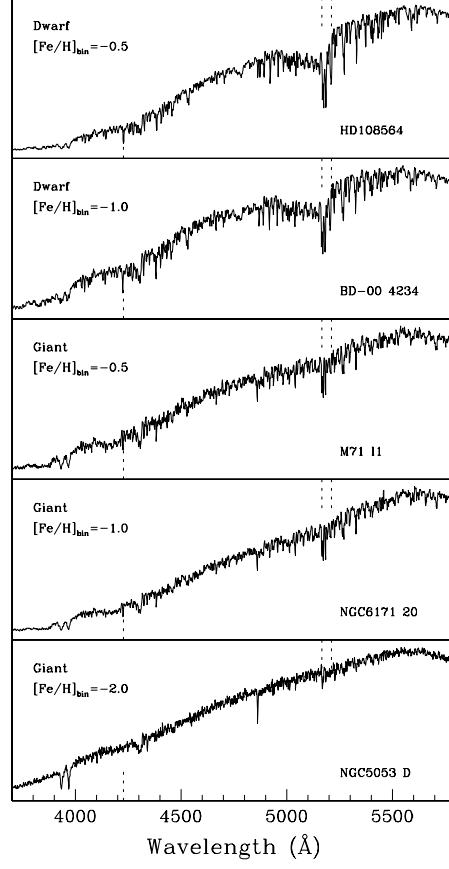


FIG. 3.—Spectra of known late-type giants and dwarfs taken on the KPNO 4 m RC spectrograph in 1999 May. Metallicity and $M - T_2$ color of star is given on each spectrum. Stars are ranked horizontally by $M - T_2$ color, with the bluest stars to the left, and by both luminosity and metallicity vertically. Dwarf spectra are shown at the top of each vertical panel and giants at the bottom, with the most metal-rich in each class at the top. The dwarfs in the bluer color range show a weak MgH feature because they are hotter than the temperatures where the MgH band is strongest. For stars with $M - T_2 > 1.10$, it can be seen that even metal-poor dwarfs have a strong MgH feature and can easily be distinguished from metal-poor giants. The MgH band head, the Mg b line at 5167 Å, and the Ca I λ 4227 line are marked.

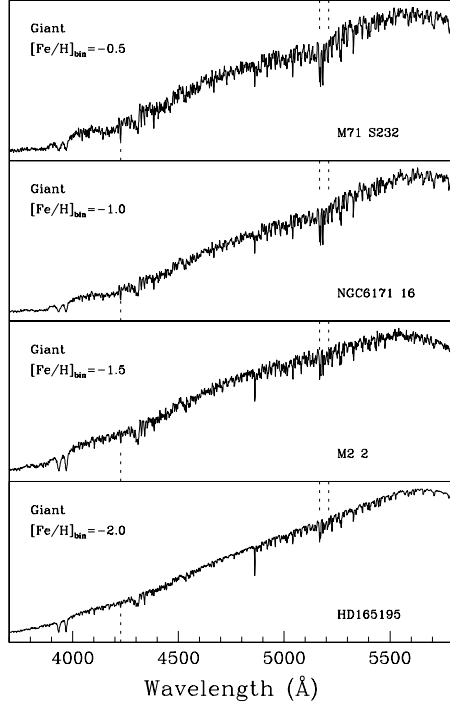
$$M-T2_{\text{bin}} = 1.20$$



$$M-T2_{\text{bin}} = 1.30$$



$$M-T2_{\text{bin}} = 1.45$$



$$M-T2_{\text{bin}} = 1.70$$

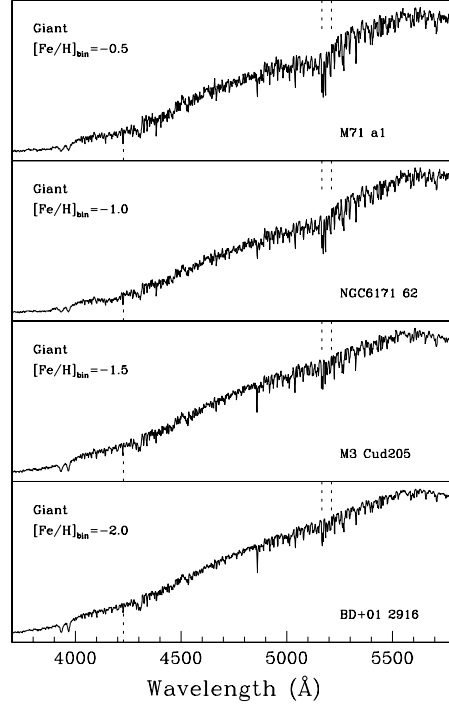


FIG. 3.—*Continued*

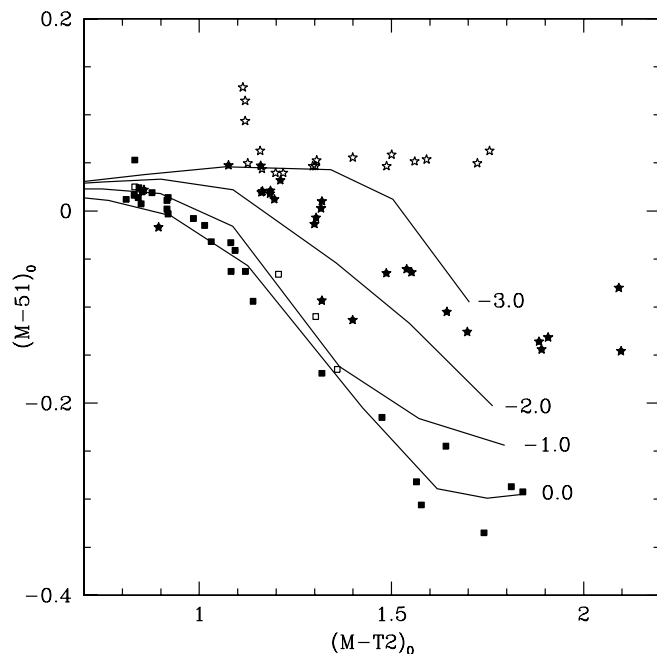


FIG. 4.— $M-51$ color for a selection of known late-type dwarfs and giants plotted vs. $M-T_2$ color. Dwarfs with roughly solar metallicity are plotted as filled squares, and those with $[\text{Fe}/\text{H}]$ between -0.5 and -1.5 as open squares; solar abundance giants are plotted as filled stars; and metal-weak giants from the globular clusters NGC 6541 ($[\text{Fe}/\text{H}] = -1.83$; Zinn 1985) and NGC 6397 ($[\text{Fe}/\text{H}] = -1.91$; Zinn 1985) are plotted as open stars. Loci traced by the dwarf models of Paltoglou & Bell (1994) for $[\text{Fe}/\text{H}]$ from 0.0 to -3.0 are also shown.

from Figure 4 that the use of $M-T_2$ as a color does not degrade the luminosity sensitivity. Our measurement errors for $M-51$ are 0.02 – 0.04 mag, allowing us to discriminate easily between giants and all dwarfs except the most metal poor using our photometric survey.

Because we are searching for intrinsically very rare objects, we are particularly vulnerable to photometric errors—dwarfs with 3σ errors in their colors are more common than our most distant halo giants. Because all but a few percent of the known halo stars have $[\text{Fe}/\text{H}] < -1.0$, we can use metallicity as an additional criterion. We use an additional Washington filter to identify halo giants: C . $C-M$ is a metallicity indicator that was calibrated for giants by Geisler, Clariá, & Minniti (1991). We require that candidates lie in the $[\text{Fe}/\text{H}] < -1.0$ region of the Washington $C-M$ versus $M-T_2$ diagram.

Figures 5 and 6 show how successful our photometric classification has been. Photometric data from 22 high-latitude fields observed at the CTIO 4 m with the BTC in 1999 April are plotted with spectroscopic confirmations shown as larger symbols. These data will be described in more detail by Dohm-Palmer et al. (2000). Note that we deliberately chose to observe candidates near the giant-dwarf boundary to mark it carefully for future work.

3.1.2. Extreme K Subdwarfs

Metal-poor halo dwarfs are of particular concern because their spectra more closely resemble metal-poor giants. The Bahcall & Soniera (1984) model predicts that 15 halo dwarfs will be found per square degree down to $V = 20$ in the color range that we search for giants ($B-V = 0.9$ to 1.2). (Recall from § 3.1 that we expect to see four to five halo giants in the same magnitude interval.)

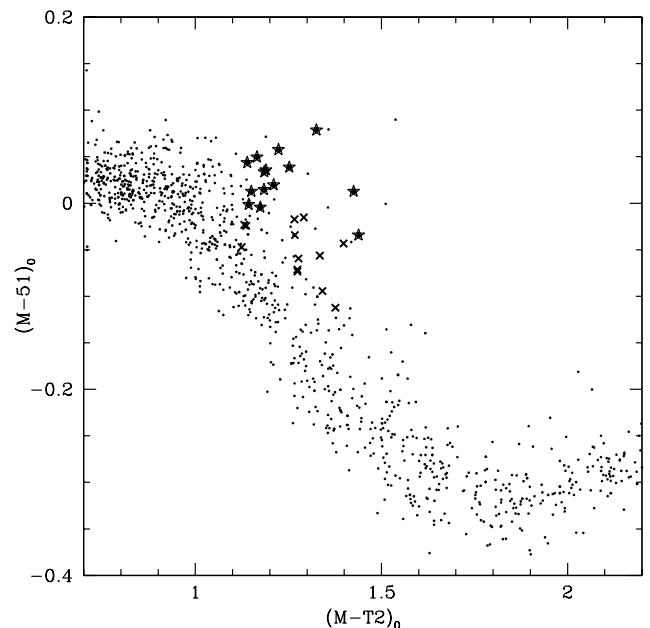


FIG. 5.—Spectroscopically confirmed halo giant stars in the $M-51$ versus $M-T_2$ diagram. Small circles are stars of all colors identified on several BTC fields, plotted to show the region where foreground dwarfs are found; crosses are halo giant candidates that were found to be dwarfs when spectra were obtained, and stars are spectroscopically confirmed halo giants. We deliberately observed stars with low $M-51$ values to delineate the dwarf region as accurately as possible.

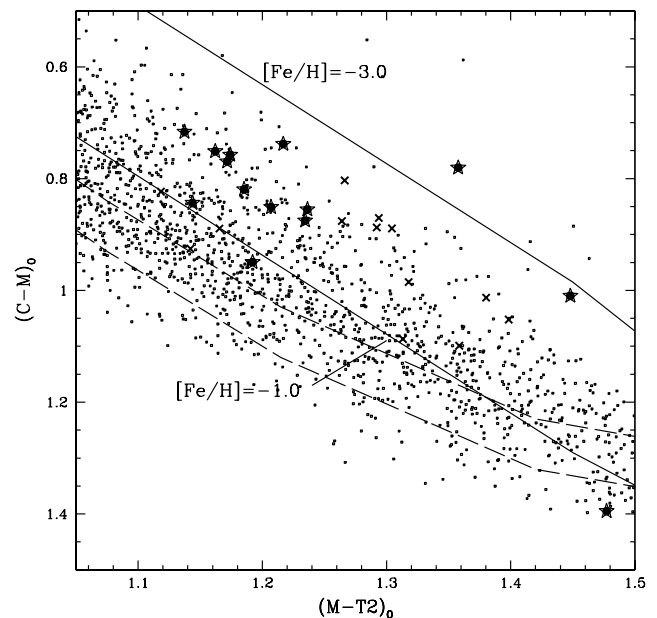


FIG. 6.—Spectroscopically confirmed halo giant stars in the $C-M$ vs. $M-T_2$ diagram. Small circles are stars of all colors identified on eight BTC fields, plotted to show the region where most foreground dwarfs are found; crosses are halo giant candidates that were found to be dwarfs when spectra were obtained; and stars are spectroscopically confirmed halo giants. Solid lines show the calibration lines for $[\text{Fe}/\text{H}] = -1.0$ and -3.0 from Geisler et al. (1991), and dashed lines show the calibration lines of Gonzalez & Piché (1992) for $[\text{Fe}/\text{H}] = 0.0$ and -0.5 . Because the metal-poor giants have a smaller separation from the dwarf sequences for cool stars, identification becomes less efficient there. It can be seen that the model prediction of roughly equal numbers of thick- and thin-disk dwarfs in our fields is borne out by our data: few stars are found below the $[\text{Fe}/\text{H}] = 0$ line for dwarfs, and there are significant numbers of stars near the $[\text{Fe}/\text{H}] = -0.5$ line. $[\text{Fe}/\text{H}] = -0.5$ should represent the mean abundance for thick-disk dwarfs.

There are very few metal-poor K dwarfs with $M-51$ photometry available, so we cannot accurately measure the photometric separation between metal-poor dwarfs and giants. However, Paltoglou & Bell (1994) have calculated synthetic $M-51$ colors for their grid of dwarf and giant models of different metallicity. These models are based on the line lists of Bell, Paltoglou, & Trippico (1994). We show their dwarf sequences for $[\text{Fe}/\text{H}]$ from 0.0 to -3.0 in Figure 4. It can be seen that the most metal-poor dwarfs, with $[\text{Fe}/\text{H}] < -2.0$, overlap the region where giants are found in this diagram. Thus, the models suggest that the $M-51$ photometric index will not be useful for weeding out the extreme K subdwarfs in our fields—we will need to examine their spectra in more detail.

How common are these extremely metal-poor subdwarfs? We can estimate the number of halo dwarfs with $[\text{Fe}/\text{H}] < -2.0$ using the halo metallicity distribution of Ryan & Norris (1991); 31% of their sample has $[\text{Fe}/\text{H}] < -2.0$, which, in conjunction with the results of the Bahcall & Soniera (1984) model, translates to four very metal-poor halo dwarfs per square degree for $V < 20$ at the NGP. Halo dwarfs only appear in significant numbers for $V > 18$, but the very distant halo giants also have $V > 18$. We need to consider these contaminants seriously.

We have approached the problem of discriminating spectroscopically between halo giants and extreme K subdwarfs in two ways—by obtaining spectra of the few extremely metal-poor K dwarfs known in this temperature range, and by supplementing these with synthetic spectra. It is practical to depend on follow-up spectroscopy to weed these objects out because of their rarity.

Because some of the major differences between K dwarfs and giants are due to molecular bands, we have used the NextGen model atmosphere grid (Hauschildt, Allard, & Baron 1999a; Hauschildt et al. 1999b) for the synthetic spectra. These models were originally designed to model the atmospheres of very low-mass stars and brown dwarfs and

include a detailed molecular equation of state and a set of molecular opacity sources that improve on those used in previous work. Hauschildt et al. (1999a) state that their models are more suitable for stars with $T_{\text{eff}} < 5000$ K than previous models such as that of Kurucz (1992).

The NextGen models are described by Hauschildt et al. (1999a, 1999b). Peter Hauschildt kindly computed NextGen models with $[\text{Fe}/\text{H}] = -2.0$ and an overabundance of the α -elements similar to that seen in halo stars ($[\alpha/\text{Fe}] = 0.4$) for us. They were calculated with $\log g = 1.0$ and 4.5 to match giants and dwarfs with effective temperatures of 4700 and 4500 K, respectively. The model spectra are shown in Figure 7, smoothed to the same resolution as our 4 m spectra. It can be seen that there are marked differences between giants and dwarfs with $[\text{Fe}/\text{H}] = -2$. Both dwarf models, especially the cooler one, show MgH features, and both show strong lines of Ca I $\lambda 4227$, unlike the giants, and much stronger Mg b lines. The dwarfs also show much stronger lines in the region blueward of the Ca H and K lines, particularly in the region near 3840 Å, where lines of Fe I and Mg I contribute.

In Figures 8 and 9, we focus on two regions of the spectrum that are particularly useful for luminosity discrimination, comparing spectra of known metal-poor dwarfs and giants and supplementing with synthetic spectra when no real spectra are available. Figure 8 shows the region between 3700 and 4500 Å. It can be seen that the most metal-poor dwarf for which we have a spectrum, HD 134440, with $[\text{Fe}/\text{H}] = -1.5$ and $T_{\text{eff}} = 4740$ K (Carbon et al. 1987), matches the model spectrum with $[\text{Fe}/\text{H}] = -2.0$ and $T_{\text{eff}} = 4700$ K quite well, giving confidence in the synthetic spectra. There is no marked difference in G-band strength between giants and dwarfs, but all the dwarf spectra show a strong feature at Ca I $\lambda 4227$. The metal-poor giants of moderate metal deficiency ($[\text{Fe}/\text{H}] \geq -1.6$) show a weaker Ca I line, while the very metal-poor giant shows almost none.

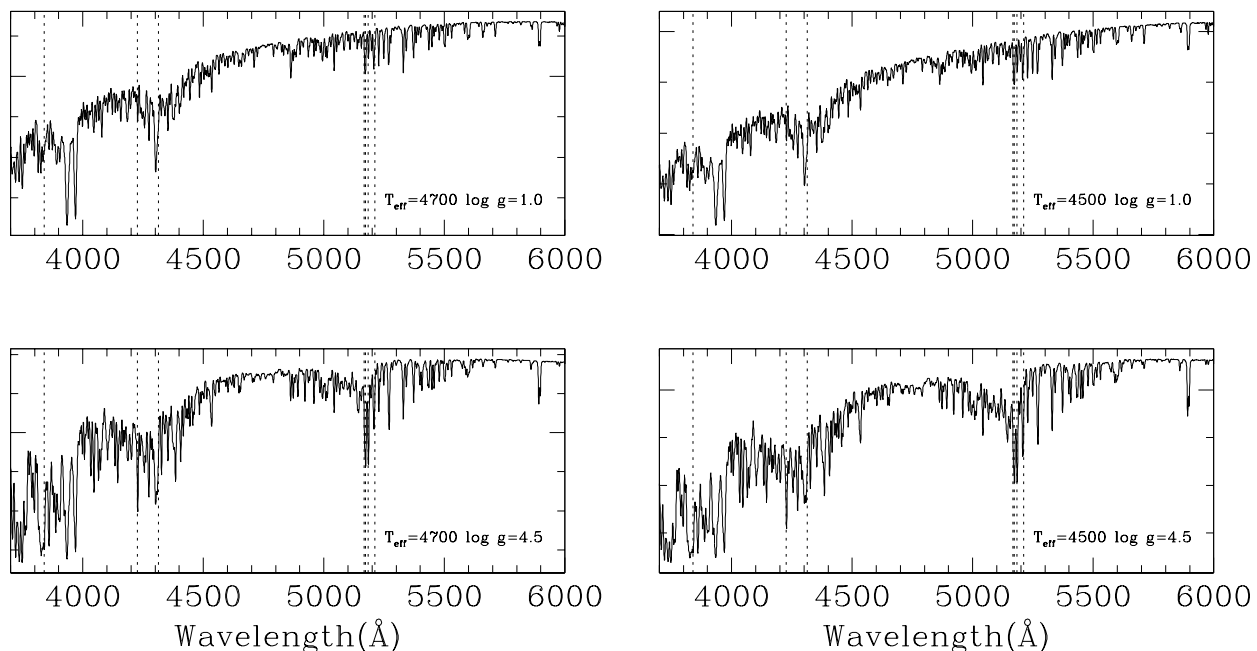


FIG. 7.—Model spectra for stars with $[\text{Fe}/\text{H}] = -2.0$, $[\alpha/\text{Fe}] = 0.4$, $\log g = 1.0$ and 4.5, and $T_{\text{eff}} = 4700$ and 4500 K. Positions of the MgH band head at 5211 Å, the Mg triplet, the G band, the Ca I $\lambda 4227$ line, and the group of Fe I and Mg I lines near 3840 Å are marked.

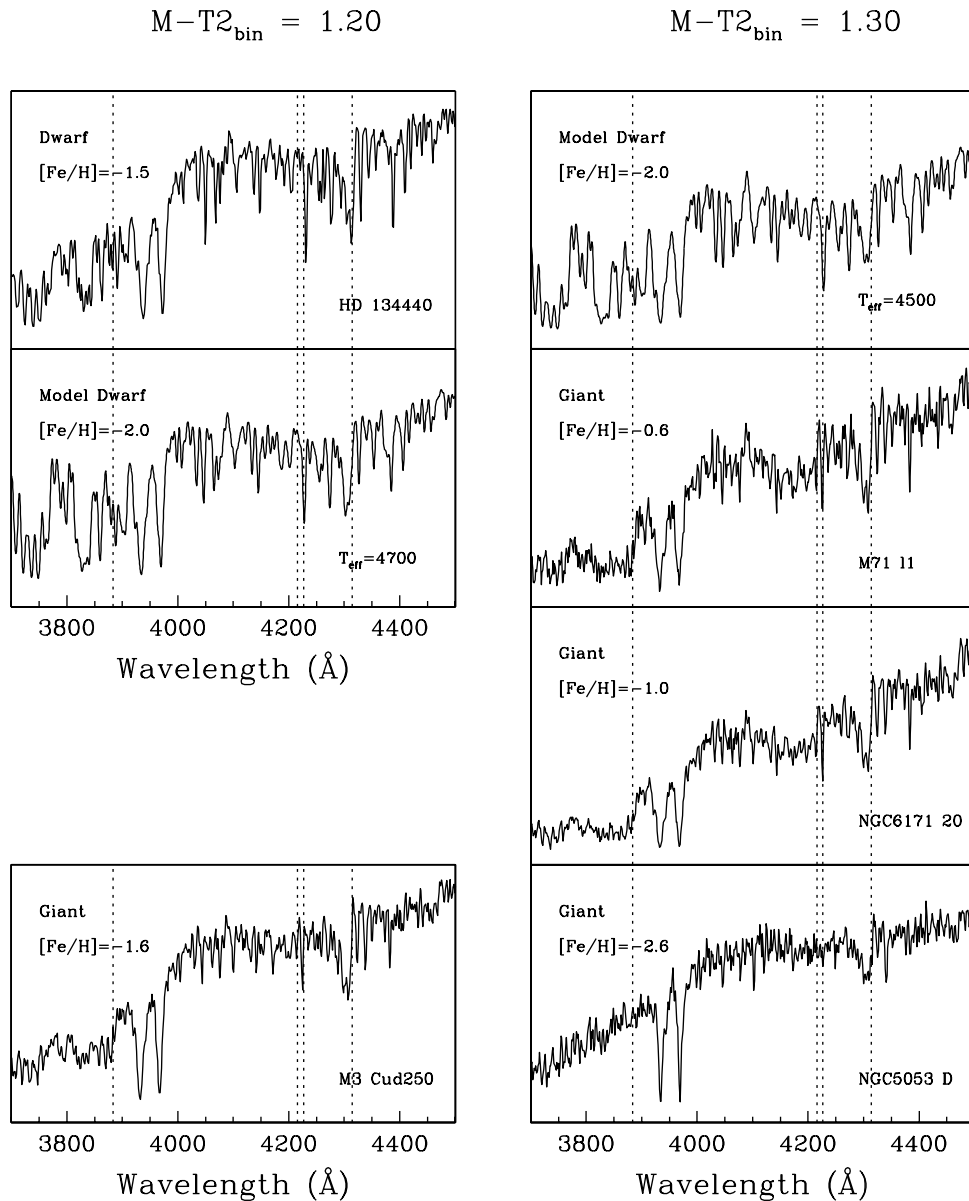


FIG. 8.—Spectra of metal-poor subdwarfs and giants of various metallicities, sorted into $M-T_2$ bins, in the spectral region from 3700 to 4500 Å. Wavelengths of the G band, Ca I 84227 line, blue CN band head, and UV CN band head are marked. HD 134440 has a radial velocity of 308 km s^{-1} , which explains why its spectral lines are offset from their rest wavelength.

The blue and UV CN bands are also visible in the giants with $[\text{Fe}/\text{H}] \geq -1.6$, while the dwarf spectra look quite different in this region. The feature just blueward of 3840 Å is very strong in the dwarfs and is significantly narrower than the UV CN band. We note that because of CN anomalies in globular clusters, the CN strength of the stars in Figure 8 may not be typical of field stars. While CN measurements of the three globular cluster giants shown in Figure 8 are not available, field giant stars do show these CN features, as can be seen in Figure 4b of Flynn & Morrison (1990). This criterion can be used as a way of confirming that a star is a giant because no dwarf shows these CN features. It cannot be used as a way of confirming that a star is a dwarf because some giants may be CN weak.

Figure 9 shows the region from 5000 to 5300 Å . While the large-scale shape of the MgH band is not easily visible when such a small region of spectrum is displayed, it can be seen

that at a given $M-T_2$ color, both the MgH band head and the Mg triplet are stronger in the subdwarfs than in any of the giants. Even the M71 giants, whose metallicity is higher than we aim to identify in our halo sample, are distinguishable from subdwarfs. However, the effect is too small to depend on the $M-51$ color to identify these subdwarfs reliably.

In conclusion, our photometric survey will weed out the more common dwarfs of the thin and thick disks, but is unable to identify the very metal-poor K subdwarfs of the halo. These stars are rare enough that it is practicable to use follow-up spectra with good S/N to reject them. We can measure our success rate for photometric preselection using the percentages of spectroscopically confirmed giants, foreground dwarfs, and subdwarfs. We found 70% of giant candidates in the correct region of the $M-51$ versus $M-T_2$ diagram were giants, 20% were subdwarfs, and 10% were

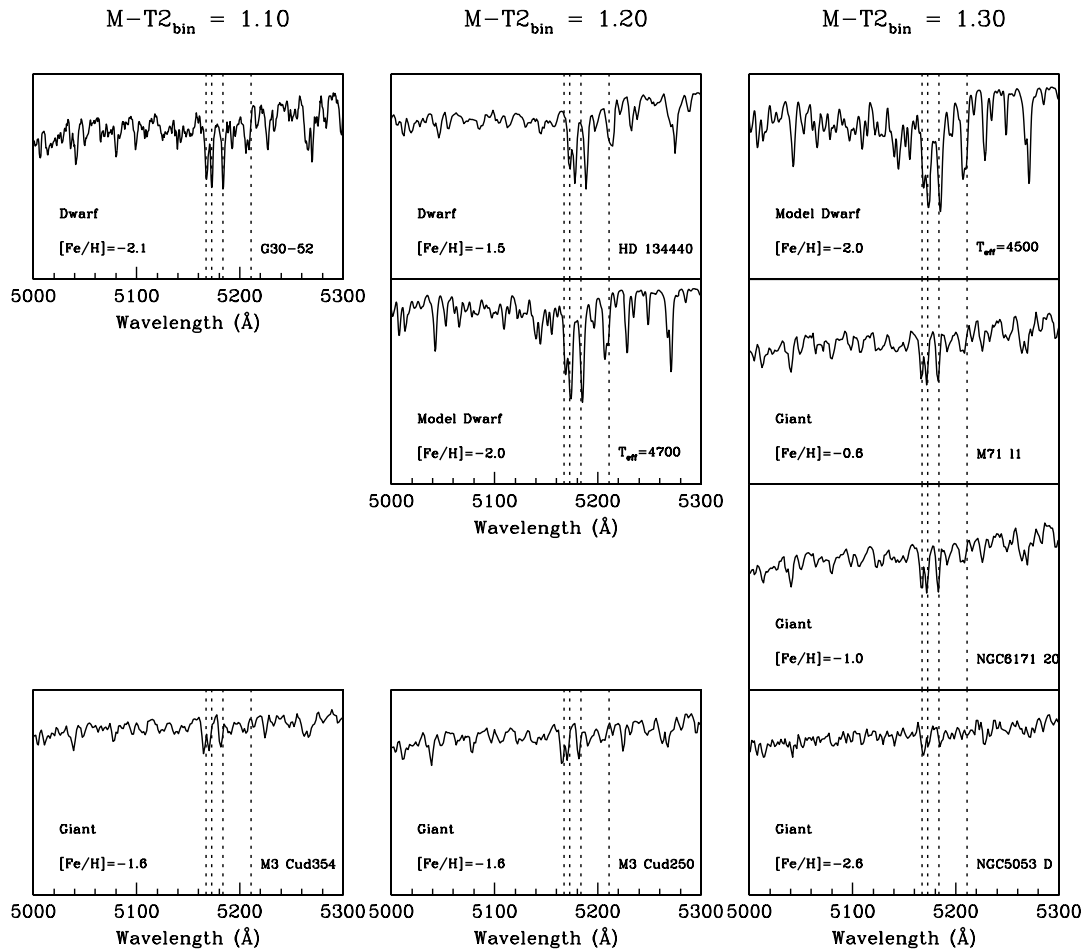


FIG. 9.—Same as Fig. 8, but in the spectral region from 5000 to 5300 Å. Wavelengths of the MgH band head at 5211 Å and the Mg triplet are marked.

dwarfs. Given our expected lack of success in discriminating subdwarfs from giants photometrically, this confirms that our photometric selection technique is very effective.

Figure 10 illustrates the success of our selection with spectra of metal-poor giants identified in our survey. Metallicity and distance values obtained from the Washington $C-M$ versus $M-T_2$ calibration are given for each star. Our sample already includes two stars that are more distant than the LMC, one of which is shown in Figure 10, and we are well placed to discover a large number of giants in the outer halo where only dwarf satellites and globular clusters were previously known.

3.1.3. Extragalactic Contaminants

Possible extragalactic contaminants of our giant sample are QSOs and unresolved galaxies. Reid & Majewski (1993) show that there are ~ 15 QSOs and unresolved galaxies per square degree down to $R = 19$ at the NGP.

Most QSOs are separable photometrically because of their unusual positions in the color-color diagram, although a few need to be weeded out spectroscopically. However, color discrimination does not work for unresolved normal galaxies, as their integrated colors are similar to those of metal-poor giants (D. Geisler 1995, private communication). The large pixels on the Schmidt Telescopes mean that we are more vulnerable to this problem there. With smaller pixels, the galaxy contamination is much less severe—on our recent 4 m run (reported by Olszewski et al.

2000), where 14 halo giants were identified from CTIO 4 m BTC data, no galaxies were mistakenly found.

3.2. Blue Horizontal-Branch Stars

These stars will cover a distance range 5–50 kpc and thus represent another important tracer of the outer halo in our survey. The number of BHB stars per square degree depends on the HB morphology of the halo field, which is not well determined for large distances from the Galaxy's center. If the halo field follows the globular clusters in having a redder HB morphology for large radii, then we would expect a few BHB stars per square degree in the magnitude range $V = 15-20$.

We restrict ourselves to the portion of the HB that is flat in V magnitude, between $B-V = 0.0$ and 0.20 . This converts to a color range $0.0-0.30$ in $M-T_2$ (see Fig. 20).

It can be seen from Figure 2 that this is a sparsely populated portion of the CMD, and the only nonhalo contaminants of our sample in this color range are white dwarfs and QSOs. There are three white dwarfs per square degree and five QSOs per square degree down to $V = 20$ in this color range (Fleming, Liebert, & Green 1986; Sandage & Luyten 1969; Reid & Majewski 1993). Both of these types of objects are easy to discriminate with even a low-dispersion, low-S/N spectrum.

We also need to be able to discriminate between halo blue stragglers (with main-sequence gravities) and BHB stars. Our follow-up spectroscopy allows us this via Balmer

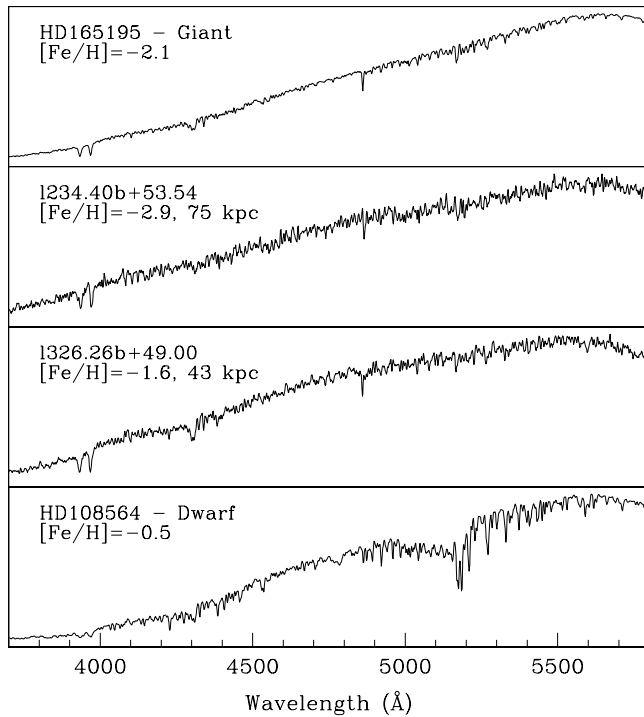


FIG. 10.—Spectra of two metal-poor red giants identified in our survey, compared with a known giant and dwarf. These spectra were obtained with the KPNO 4 m RC spectrograph in 1999 May and will be described more fully by Olszewski et al. (2000). The star name gives its Galactic longitude and latitude. The metallicity and distance of the stars are given.

line profiles (Pier 1983; Sommer-Larsen & Christensen 1985; Norris & Hawkins 1991; Kinman, Suntzeff, & Kraft 1994). In cases where we are able to obtain spectra that reach below the Balmer jump, its size can also be used as a discriminator. Kinman et al. (1994) used spectra of 3.7 Å resolution (very similar to our 4 m spectral resolution) to make this measurement. Figure 11 shows spectra of known BHB standards and two BHB stars from our sample.

3.3. Halo Turnoff Stars

Halo turnoff stars are the most numerous but least luminous tracers we shall use, and sample distances from 2–16 kpc from the Sun (assuming an absolute magnitude $M_V = 4.5$ and a limiting magnitude of $V = 20.5$). We used the halo turnoff luminosity function calculated in § 4.1 and the preferred halo model from § 4 (power-law exponent of -3.0 and an axial ratio of 0.6) to calculate the numbers of turnoff stars per square degree we would expect to see in our fields. Under these assumptions, there should be 150 halo turnoff stars per square degree down to $V = 20.5$ at the NGP, and 130 per square degree in the anticenter at $b = 45^\circ$.

These stars are relatively easy to identify using accurate photometry because they are bluer than almost all stars at

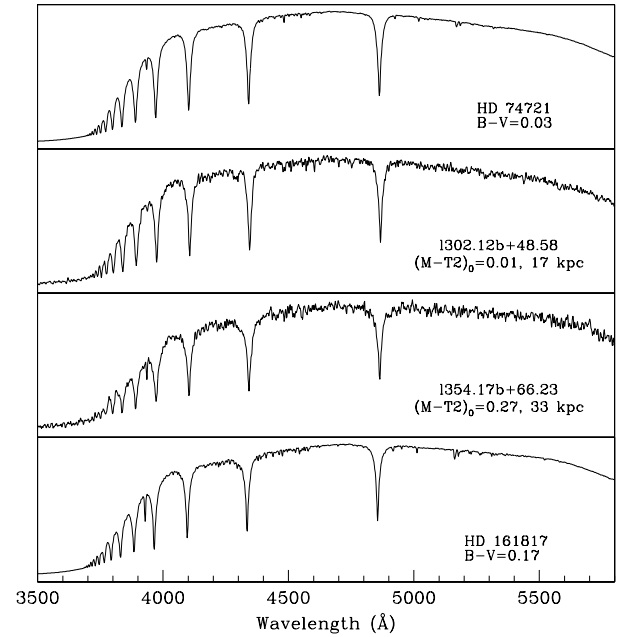


FIG. 11.—Spectra of BHB stars identified in our halo fields, compared with spectra of known field BHB stars. Stars are plotted in order of decreasing temperature. These data will be described more fully by Olszewski et al. (2000).

high Galactic latitude. For the most metal-poor globular clusters such as M92, the turnoff is at $B - V = 0.38$, significantly bluer than the turnoff color of the thick disk ($B - V = 0.5$; Carney, Latham, & Laird 1989). The thin disk has a sufficiently small scale height that very few young, thin-disk stars are found in our magnitude range at high Galactic latitude (Bahcall & Soniera 1984). We choose stars with $B - V$ color of 0.38–0.49 as halo turnoff star candidates.

The transformation to $M - T_2$ color is complicated by the fact that we have no observations of metal-poor turnoff stars in this color. We approach the problem in two ways. First, only the most metal-poor stars will have a turnoff color as blue as $B - V = 0.38$, so we could use the synthetic colors of Paltoglou & Bell (1994) for their models with $[Fe/H] = -2.0$ to derive the transformation. This predicts a turnoff color of $M - T_2 = 0.6$. Second, we can derive the turnoff color using $V - I$ and Stromgren photometry of metal-poor globular clusters from the literature. Table 3 summarizes the turnoff colors in $V - I$ and $b - y$ of metal-poor globular clusters NGC 6397, NGC 7099, and M92 and the metal-rich cluster 47 Tucanae. The average $V - I$ turnoff color for these three metal-poor clusters is 0.51, which transforms via Figure 19 to $M - T_2 = 0.64$. Thus the estimates from theory and observation are in reasonable agreement, and we have chosen to use the observational estimate here. We also use the $V - I$ photometry of Kaluzny et al.

TABLE 3
TURNOFF COLORS FOR GLOBULAR CLUSTERS

Cluster	$(b - y)_0$	$(V - I)_0$	Reference
M92	0.531	Johnson & Bolte 1998
NGC 7099	0.485	Sandquist et al. 1999
NGC 6397	0.294	...	Anthony-Twarog, Twarog, & Suntzeff 1992
47 Tuc	0.70	Kaluzny et al. 1998

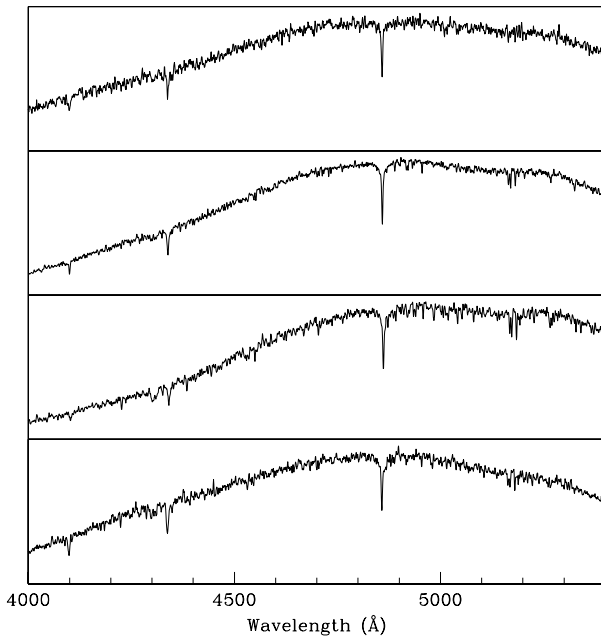


FIG. 12.—WIYN Hydra spectra of main-sequence turnoff stars identified in our halo fields.

(1998) for 47 Tuc to constrain the turnoff color of the thick disk to be $M - T_2 = 0.81$. In summary, we take the color range from $M - T_2 = 0.64$ – 0.80 for our halo turnoff stars. As a consistency check on our photometry, we also require that $C - M$ is in the range 0.2 – 0.5 .

Thick-disk stars scattering into the color range should be a minor problem because of our small photometric errors (our $M - T_2$ errors are less than 0.02 mag at $V = 19$) and the fact that we work faint enough to be away from the regions of the Galaxy where the thick disk dominates. Using the models of turnoff stars in the thick disk and halo of § 3.1, we can show that only for the brightest part of our magnitude range ($V = 16$ – 17 , corresponding to distances of order 2.5 kpc, saturated on 4 m BTC data but not on Schmidt data) are numbers of thick-disk stars per square degree greater than halo star numbers in our fields, and then only by a factor of ~ 2 , which is not large enough to make significant numbers of thick-disk stars “leak” into the halo color range via photometric errors. For stars with $V = 17$ – 18 , numbers of thick-disk and halo turnoff stars are approximately equal, and for fainter magnitudes, halo turnoff stars outnumber thick-disk stars.

The only other contaminants of our sample in this color range are small numbers of white dwarfs, QSOs, and RR Lyraes. The QSOs and white dwarfs are obvious from spectra, and the RR Lyraes are sufficiently rare that few will

be detected and some of these will be removed because of their variability on either photometric or spectroscopic observations.

Figures 2 and 14 illustrate the selection technique, showing CMDs ($M - T_2$ vs. M) for a single field and for a composite of many fields. The position of the turnoff for both halo and thick disk is marked, and our candidate halo turnoff stars are shown. With very few exceptions, all stars in this region of the CMD show spectra typical of halo stars, i.e., metal poor. Figure 12 shows WIYN Hydra spectra of several of these stars. It is clear that the halo turnoff candidates are indeed metal poor, confirming the accuracy of our photometry.

3.4. Blue Metal-Poor Stars

Preston et al. (1994) identified an important group of halo turnoff stars with color bluer than $B - V = 0.38$ and suggested that these stars were metal-poor stars with unusually young ages that had originated in dwarf spheroidal satellites that were subsequently accreted into the Galaxy’s halo. Another possibility is that these stars are the result of the evolution of multiple star systems of the halo. Preston has obtained detailed follow-up spectroscopy of a number of these stars to test this possibility. Preston et al. (1994) estimated numbers in the solar neighborhood of 350 – 450 per kpc^3 (cf. the density from Table 4 of 2695 halo turnoff stars per kpc^3 with $M_V = 4.5$). Unavane, Wyse, & Gilmore (1996) found from photographic star-count data that $\sim 10\%$ of halo stars were bluer than $B - V = 0.4$, which is in rough agreement with the Preston et al. (1994) value. These BMP stars are particularly important for our survey if they have younger ages, and we select them by $B - V$ color between 0.15 and 0.35 ($M - T_2 = 0.2$ to 0.6).

Using the Preston et al. (1994) local normalization, we expect to find 10 – 20 BMP stars per square degree to $V = 19$. Our Figure 2 shows 23 such stars in the color range $M - T_2 = 0.2$ – 0.6 for an area of 2.75 deg^2 , a little lower but not significantly different from the value of Preston et al. (1994).

4. MAPPING THE HALO: “INTELLIGENT” STAR COUNTS

Accurate CCD photometry of large areas in many fields makes a new method of investigation of the halo possible. As discussed in § 3.3, the halo turnoff color is $B - V = 0.38$, and the thick-disk turnoff is $B - V \sim 0.5$, so stars with colors between these two numbers are almost certainly halo stars close to the turnoff. Photographic colors have such large errors (0.05 – 0.10 mag) that it is not possible to isolate halo turnoff stars from photographic data without simultaneously modeling the contribution of the thick disk. In contrast, our photometry is of such high and uniform quality that it is possible to separate halo turnoff stars cleanly from thick-disk turnoff stars using the $M - T_2$ color. Figure 14 illustrates this in one of our lowest latitude fields, where both thick-disk and halo turnoffs can be seen.

We now make a preliminary analysis of the BTC data to illustrate the power of our survey technique. The data set obtained with the BTC on the CTIO 4 m telescope in 1999 April (Dohm-Palmer et al. 2000) is particularly useful for mapping the halo because of the uniform quality of the data and the fact that conditions were photometric throughout the run. Figure 13 shows in cartoon form the location of the fields where data were obtained. There are 46 fields with latitudes ranging from 25° – 73° and longitudes from $l = 17^\circ$

TABLE 4

HALO TURNOFF STAR LUMINOSITY FUNCTION FOR STARS WITH $B - V$ BETWEEN 0.38 AND 0.50

M_V	Φ (stars per kpc^3)	Number of Stars in Carney et al. Sample
3.5.....	73.1	2
4.0.....	986.0	13
4.5.....	2695.7	46
5.0.....	807.8	17
5.5.....	151.2	5

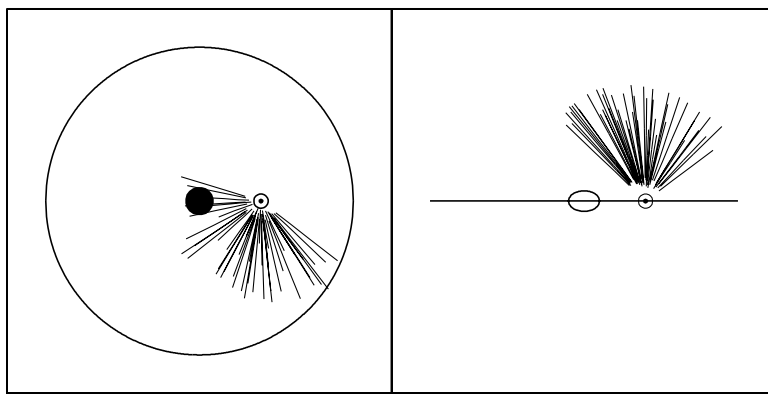


FIG. 13.—Face-on (*left*) and edge-on (*right*) views of the Galaxy with the lines of sight traced by the 46 BTC fields shown. The position of the Sun, Galactic center, and edge of disk at $R = 20$ kpc are shown.

through the Galactic center to $l = 218^\circ$ (less than 40° from the anticenter).

We have checked for errors in reductions or reddening estimation by carefully examining the CMDs of all fields. Figure 14 is typical: the position of the halo turnoff is clear and agrees well with the calculated value of $(M - T_2)_0 = 0.64$ in all but two of the 46 fields. In these two fields, it appears that the Schlegel reddening values that we used should be adjusted by a few hundredths in order to bring the turnoff position to this color. Because the stars are uniformly distributed across the color range from $(M - T_2)_0 = 0.64$ to $(M - T_2)_0 = 0.8$, photometric errors or reddening estimates of a few hundredths of a magnitude will in no case be strong enough to make the turnoff star numbers vary significantly.

Models of the shape of the halo have in many cases been derived from easily detectable tracers such as globular clus-

ters (Zinn 1985) or HB stars (Kinman et al. 1965; Saha 1985; Hartwick 1987; Preston, Shectman, & Beers 1991; Kinman et al. 1994). Studies using star counts (e.g., Bahcall & Soniera 1984) are handicapped by their inability to separate the halo and thick disk accurately with photographic photometry, as discussed above. Models from both globular clusters and field stars both find that the halo is centrally concentrated, with the power-law exponent varying from -3.0 to -3.5 or even steeper. Axial ratios vary from 0.5 to 1.0 , with suggestions from several groups that the axial ratio might change with Galactocentric radius in the sense that the outer halo is spherical and the inner halo flattened.

However, neither globular clusters nor HB stars are ideal for measuring the density distribution of the halo. First, it is not clear that the halo field stars were formed under the same conditions as the globular clusters. Second, possible age and metallicity gradients in the halo (Searle & Zinn 1978; Zinn 1993; Preston et al. 1991; Kinman et al. 1994) are reflected in HB morphology. This causes a different power-law exponent to be derived for RR Lyrae and BHB stars, as found by Preston et al. (1991). Thus a check of the earlier results with a different tracer is valuable. Although our turnoff star sample will also be sensitive to age and metallicity variations, we are able to check for such effects by examining the CMDs of discrepant fields directly.

4.1. Local Halo Density

The estimation of the halo density in the solar neighborhood is even more challenging than the measurement of its density in more distant fields. It has in most cases been based on the local density of stars selected by their high proper motion (e.g., Bahcall & Casertano 1986), with kinematic corrections made for the amount of the halo that would be missed using this selection technique. There have also been a small number of direct measurements of local density of some tracer such as RR Lyraes or red giants (e.g., Preston et al. 1991; Morrison 1993) that agree within a factor of 2 with the proper-motion data, but different selection effects such as metallicity operate for these samples. Attempts to extrapolate the results of pencil-beam surveys inward to the solar neighborhood are not always successful—Preston et al. (1991) and Wetterer & McGraw (1996) note the disagreement of a factor of 2 between the counts of nearby RR Lyrae variables and the extrapolation of more distant RR Lyrae counts inward.

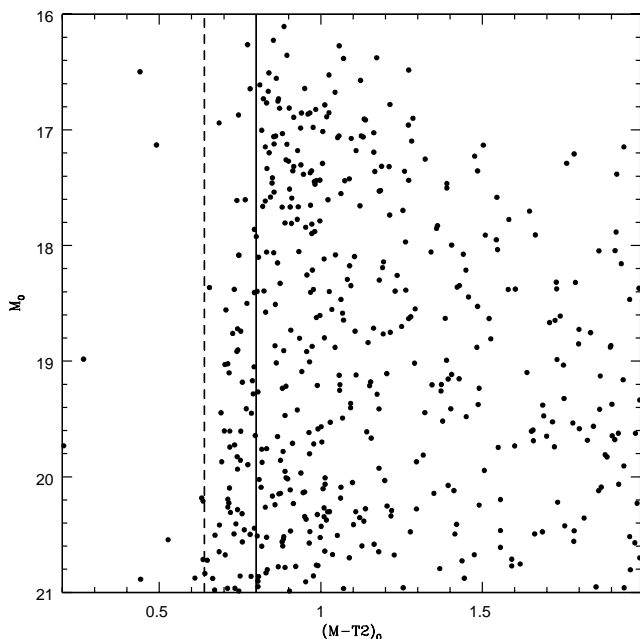


FIG. 14.—CMD of a field at $l = 234^\circ$, $b = 32^\circ$, with position of halo turnoff (*dashed line*) and thick-disk turnoff (*solid line*) shown. The thick-disk stars are clearly visible redward of the solid line for M brighter than 18. Halo turnoff stars are rare for these brightnesses and become increasingly common for fainter values of M .

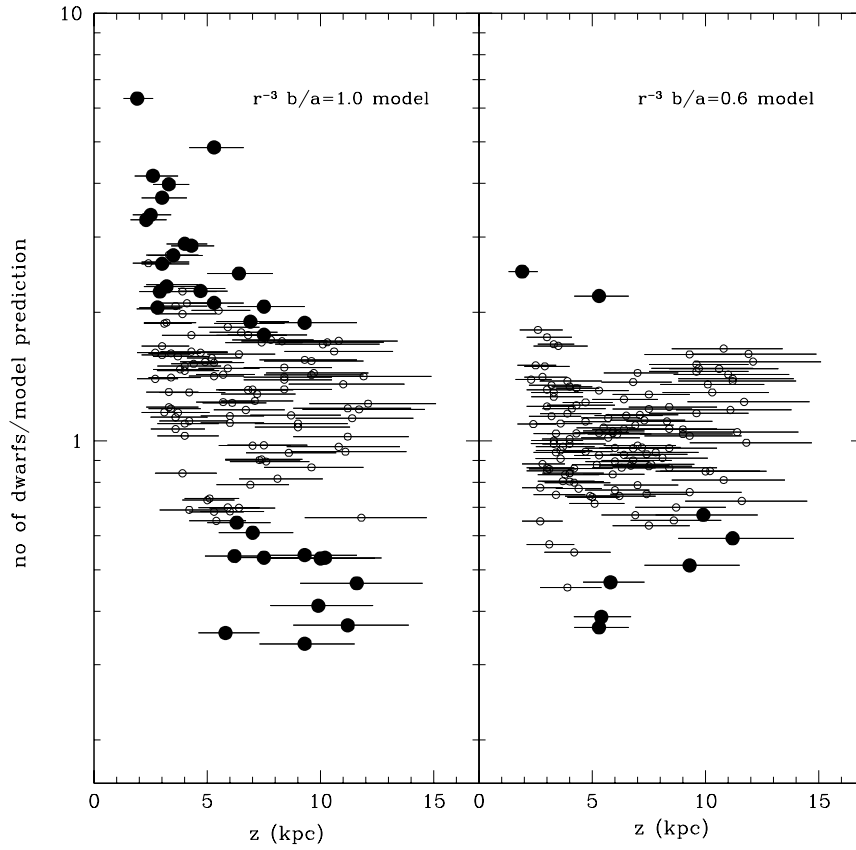


FIG. 15.—Ratio of number of turnoff stars to model prediction vs. the range of z -heights traversed. Points that are more than 2.5σ from the model are shown as solid symbols. The local halo density was adjusted to give the best fit for these fields: the spherical halo model uses a local density 40% of that given in Table 4, and the halo with $b/a = 0.6$ has a local density 10% higher than that of Table 4.

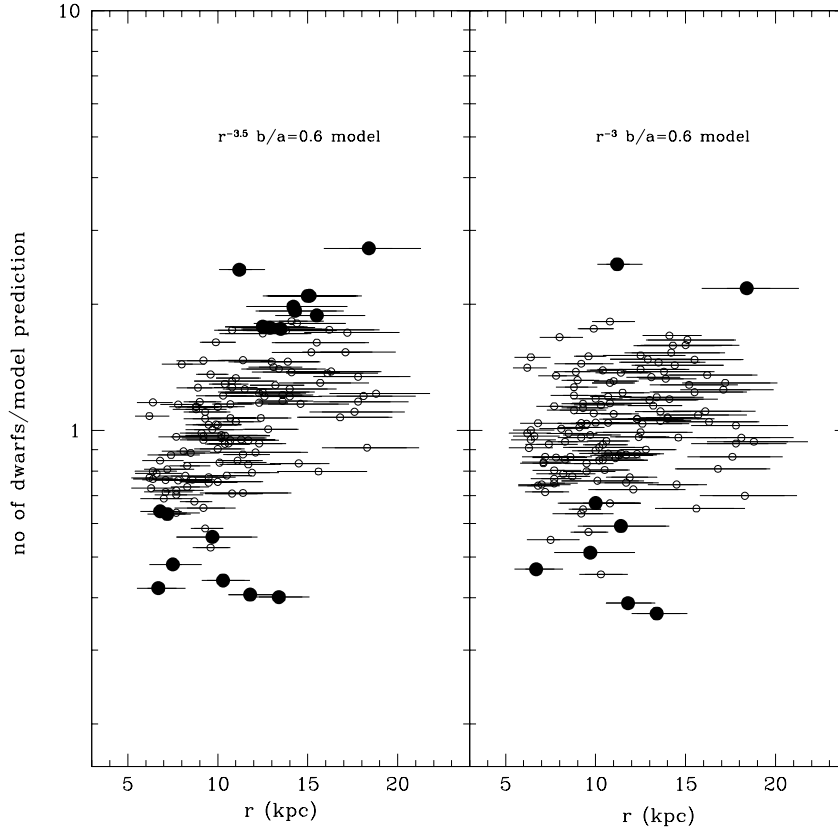


FIG. 16.—Same as Fig. 15, but vs. the range of R_{gc} values traversed by the line of sight. The model with exponent -3.5 uses a local density 40% larger than that given in Table 4 while the halo with exponent -3.0 has a local density 10% higher than that of Table 4.

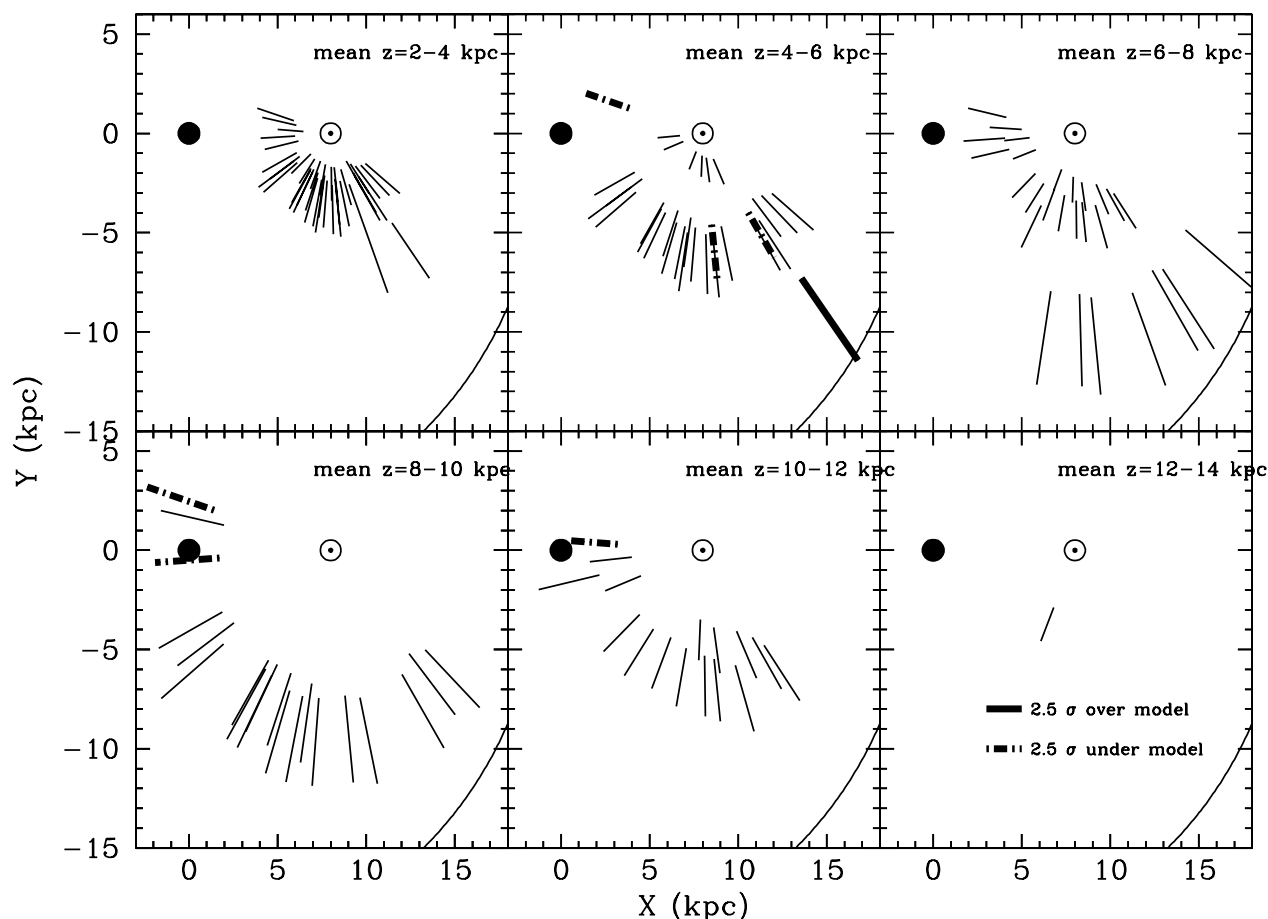


FIG. 17.—Face-on views of the Galaxy for different ranges of z -height. Lines of sight whose halo turnoff star numbers agree with our model are shown as solid lines. Lines of sight that are more than 2.5σ above the model are shown as thick lines, and those that are more than 2.5σ below are shown as dashed lines.

Since we have few low-latitude fields and our BTC data saturate for magnitudes much brighter than $V = 17$ (corresponding to a distance of 3 kpc for turnoff stars), we have no direct constraints on the local density from our data. Our preferred value of the solar neighborhood halo density will depend on the axial ratio adopted.

We decided to reexamine the measurement of the local halo density from the proper-motion samples, as there have been significant advances in the information available on these stars since the work of Bahcall & Casertano (1986). We have used the extended sample of Carney et al. (1994), which has been updated recently to have a distance scale consistent with the *Hipparcos* parallax measurements for subdwarfs, to make an estimate of the local density. Bruce Carney kindly made this sample available to us in advance of publication. Also, in order to make comparisons with our BTC data easier, we isolated stars in the turnoff star color bin we used ($B - V$ between 0.38 and 0.5, corresponding to $M - T_2$ between 0.64 and 0.8) and then derived a local luminosity function for these stars alone. Because this is a kinematically selected sample, we need to make corrections for the halo stars missed because of the proper-motion selection. To minimize contamination of the sample by thick-disk stars, which contribute strongly to the derived local density because the lowest velocity stars are given the highest weights (see Bahcall & Casertano 1986), we only used stars with tangential velocity greater than 220 km s^{-1}

and rejected all stars with $[\text{Fe}/\text{H}] > -1.0$. This may reject a few genuine halo stars but will cause an error of only $\sim 10\%$ in the derived density (Carney et al. 1989). Erroneously including thick-disk stars would have a much larger effect.

The Carney et al. (1994) sample is drawn from the Lowell Proper Motion Catalog that covers the entire northern hemisphere and has a proper-motion lower limit of $0''.26 \text{ yr}^{-1}$. In the color range of concern here, the catalog's magnitude limit is sufficiently faint that all we need to do is correct for proper-motion selection effects, which we do by weighting by V_{tan}^{-3} , following Bahcall & Casertano (1986). Table 4 gives our results. Carney and collaborators have a more complete kinematic analysis in progress, so we have chosen simply to use the simulations of Bahcall & Casertano (1986) to correct for the tangential velocity cut at 220 km s^{-1} . Morrison (1993) notes that the sample used by Bahcall & Casertano (1986) to derive halo kinematics was probably contaminated by thick-disk stars and calculates that the “discovery fraction” for a sample with this V_{tan} cutoff should be close to 0.5, not 0.33 as they found. We have used this higher value in our calculations of the turnoff star luminosity function.

4.2. Halo Concentration and Axial Ratio

While our maps of the halo based on accurate CMDs are less sensitive to possible variations in age and metallicity

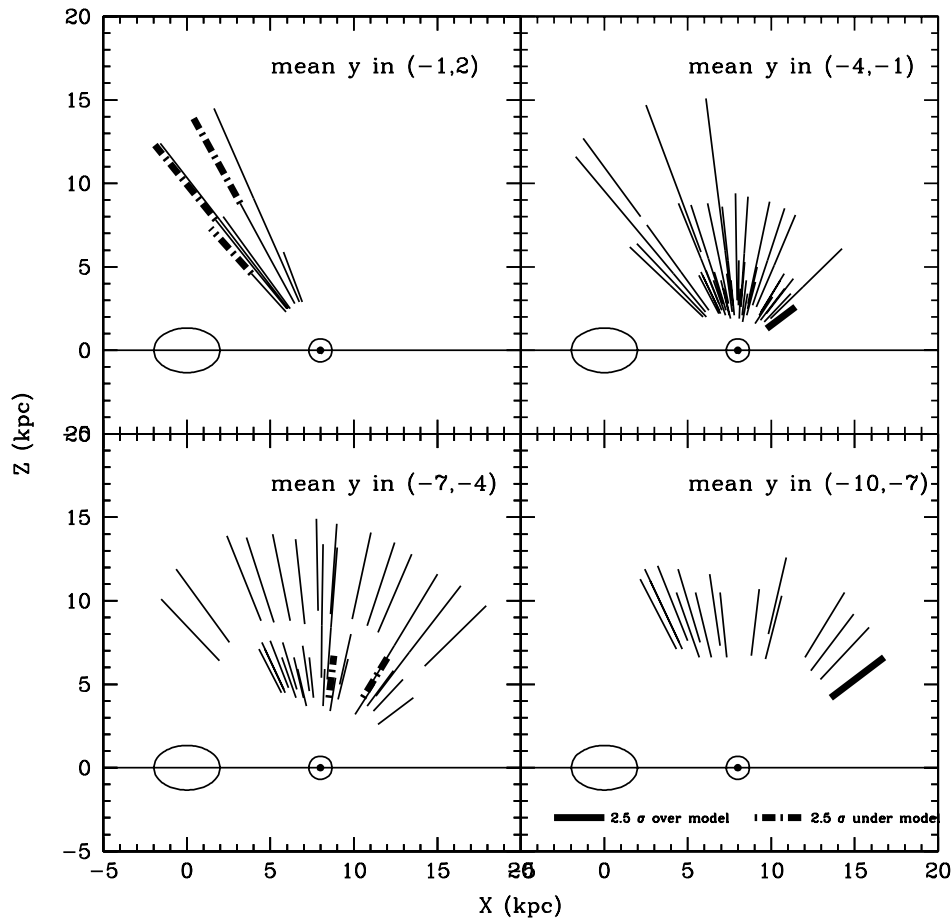


FIG. 18.—Edge-on view of the lines of sight of the 46 BTC fields. Symbols have the same meaning as in Fig. 17.

than the estimates from HB stars in particular, they are less easy to interpret because of the difficulty of obtaining accurate distances to turnoff stars. Turnoff stars in our chosen color range can have absolute magnitudes that vary from 3.5 to 5.5, although the luminosity function of Table 4 shows that many will have absolute magnitude near 4.5. We have chosen to divide our data into three magnitude ranges ($V = 17\text{--}18.5$, $18.5\text{--}19.5$, and $19.5\text{--}20.5$) and to calculate model predictions for these magnitude ranges to compare directly with the star counts there. We plan to do a more statistically sophisticated analysis in a future paper—the values we derive here will be roughly correct for the distance ranges probed by the data but may not be optimal.

Figure 15 shows the sensitivity of our data to the axial ratio of the halo. It shows the ratio of number of stars in a given magnitude bin to the model predictions. Both models have a power-law exponent of -3.0 , and one has an axial ratio $b/a = 1.0$ (spherical) while the other has a moderate flattening ($b/a = 0.6$). We have plotted these ratios versus an indicator of the z -height traveled by each line of sight, calculated by assuming that all stars in the bin have absolute magnitude $M_V = 4.5$. It can be seen in Figure 15 that the spherical halo provides a significantly worse fit. There is a trend with z : points with high z have fewer stars than the model predicts, and points with low z have more. The $b/a = 0.6$ model residuals show little trend with z , and the small number of very discrepant points remaining are found with both small and large z .

Figure 16 shows the same data/model ratios against the range in R_{gc} , for models with $b/a = 0.6$ and power-law exponent -3.0 and -3.5 . A trend with R_{gc} is visible in the panel with power-law exponent of -3.5 . The model predicts too few stars with large R_{gc} and too many with small R_{gc} . Note also that in the panel showing residuals from the model with exponent -3.0 , the remaining residuals show no clear trend with R_{gc} . We adopt a model with $b/a = 0.6$ and power-law exponent -3.0 for the rest of this analysis. Only a 10% upward correction to the local halo density of Table 4 is needed with these parameters.

It is possible to examine the residuals to the model fits in more detail by plotting the position in the Galaxy traversed by each field and highlighting the fields with large residuals. Figures 17 and 18 show a number of vertical and horizontal slices through the Galaxy, for different ranges of y and z , respectively. Fields with residuals more than 2.5σ from the model fit are highlighted. It can be seen that four of the fields with large negative residuals are toward the Galactic center, and two, with large positive residuals, are in our lowest latitude field, which is close to the anticenter. Interestingly, the discrepant fields cover a large range in both r and z , so a simple adjustment to the power-law exponent or flattening will not improve things.

The variable axial ratio models of Hartwick (1987) and Preston et al. (1991) will not solve the problem completely. The model of Preston et al. (1991) has an axial ratio changing linearly from $b/a = 0.5$ at the Galactic center to b/a

$a = 1.0$ for ellipsoids with semimajor axis of 20 kpc. While the results in fields close to the minor axis that currently have large negative residuals may be improved by the adoption of a model where the axial ratio is closer to 1 at this point, the anticenter fields will become more discrepant since the axial ratio must become close to 1 at this distance from the center too. However, it is possible that the thick disk might be partially responsible for the excess of stars in this color range, if its scale height increases in the outer Galaxy and/or it has a strong abundance gradient. We plan to investigate these issues further when we obtain more fields with low values of R_{gc} and z .

5. CONCLUSIONS

We describe a survey designed to find field stars from the Galactic halo in large enough numbers to provide a strong test of the question, Was the Galactic halo accreted from satellite galaxies? The survey will cover 100 deg^2 at high Galactic latitude. It uses an efficient preselection technique based on the Washington photometric system to identify halo red giants, BHB stars, blue metal-poor main-sequence stars, and turnoff stars. Follow-up spectroscopy (with multi-object spectrographs for the more numerous turnoff and BMP stars) tests for kinematic signatures of accretion. Our sample of halo stars will be unprecedentedly large and cover Galactocentric distances from the solar circle to more than 100 kpc. Because the photometric selection has few and easily quantifiable selection effects, our sample will also enable thorough studies of the density distribution of the Galactic halo, increasing the numbers of distant halo objects known by an order of magnitude. This will allow much more accurate measurement of the mass of the Galaxy than previously possible.

We discuss the particular problems caused for identification of the very distant halo giants by foreground K subdwarfs with very low metallicity ($[\text{Fe}/\text{H}] < -2.0$). These stars are roughly as numerous as the genuine halo giants for $V > 18$ and are not distinguishable from giants via the Washington $M-51$ filter that we use for photometric luminosity discrimination. However, with low-dispersion spectra of $S/N = 15$ or more, a combination of several spectral features such as the Ca I line at 4227 \AA suffices to distinguish these stars reliably from giants. Studies that use giants in the outer halo need to take particular care to eliminate these extreme K subdwarfs.

We use one of our large photometric data sets, obtained in one run using the BTC on the CTIO 4 m telescope, to constrain the spatial distribution of the Galaxy's halo over ranges of Galactocentric distances from approximately 5–20 kpc and z -heights from 2 to 15 kpc by using halo turnoff star numbers. We find that a power law with exponent -3.0 and a moderate flattening of $b/a = 0.6$ gives a good fit to most of the data. However, there are a number of fields that show departures from this model, suggesting that we will need a more complex model in the future as our coverage of fields in the halo increases.

It is a pleasure to thank Peter Hauschildt for kindly running the α -element-enriched NextGen models for us and making the NextGen models so readily available on the Web. We would also like to thank Doug Geisler for the careful work he has devoted to making the Washington system so useful and for his help with our many questions about the system, and Bruce Carney for kindly making his

database available in advance of publication. We have benefited from helpful discussions with Mike Bessell, Bruce Carney, Conard Dahn, and Peter Dawson. We would also like to thank an anonymous referee for comments that improved this paper. This work was supported by NSF grants AST 96-19490 to H. L. M., AST 95-28367, AST 96-19632, and AST 98-20608 to M. M., and AST 96-19524 to E. W. O. This research has made extensive use of the SIMBAD database, operated at CDS, Strasbourg, France.

APPENDIX

CONVERSIONS BETWEEN WASHINGTON AND OTHER SYSTEMS

The Washington broadband photometric system (Canterna 1976; Harris & Canterna 1979; Geisler 1996) includes the T_2 filter (which is very similar to the Cousins I filter), the M filter (which is 1050 \AA wide and has a central wavelength of 5100 \AA , slightly blueward of the V filter), and the C filter (which is 1100 \AA wide, centered near the Ca K line at 3934 \AA). Geisler (1984) has added the DDO “51” filter to make giant-dwarf discrimination possible for G and K stars. (The system also includes the T_1 filter, similar to the Cousins R filter, which we do not need to use).

The original temperature indicator for the Washington system was the $T_1 - T_2$ ($R - I$) color. However, an alternative is the $M - T_2$ color, which transforms well to $V - I$ as can be seen in Figure 19. For $V - I$ between 0.5 and 1.5, the simple linear relation $M - T_2 = 1.264 (V - I)$ works well. The standard deviation of the residuals from this line is 0.025 mag.

In Figure 19, we have included both dwarfs and giants and a significant number of metal-poor globular cluster

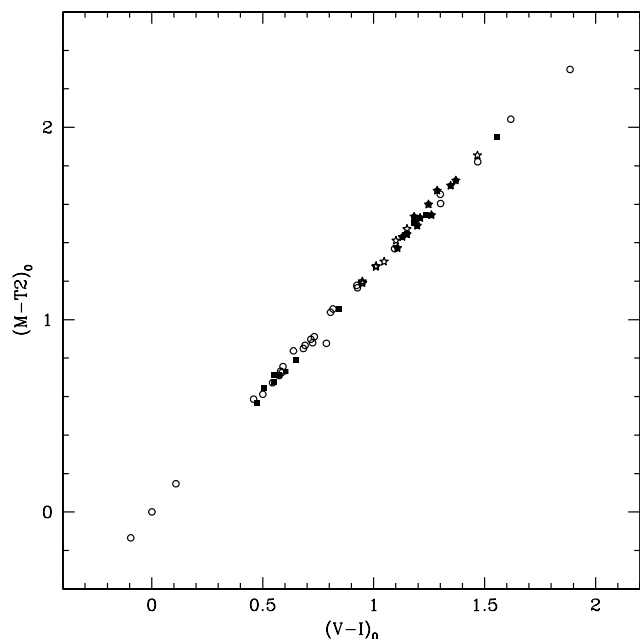


FIG. 19.—Relation between $M - T_2$ and $V - I$ for Landolt-Washington standards (giants plotted as stars, dwarfs as squares, unknown spectral types as circles) and globular cluster giants (filled stars). It can be seen that there is a simple relation between Washington $M - T_2$ color and $V - I$ and that the relation does not depend on metallicity.

giants. We used the following:

Landolt standard stars, which are also Washington standards (Landolt 1992; Harris & Canterna 1979; Geisler 1984, 1986, 1990, 1996; Geisler et al. 1991; Geisler, Minniti, & Clariá 1992). Only stars with $E(B-V)$ less than 0.11 mag, from the reddening maps of Schlegel et al. (1998), are shown. We corrected the colors using the relations between $E(B-V)$ and the extinction in the Washington passbands using the ratios from Harris & Canterna (1979).

Photometry of stars from three globular clusters: 47 Tuc, NGC 1851, and NGC 6752. The $V-I$ photometry is from Da Costa & Armandroff (1990), and the Washington photometry is from Geisler (1986) and Geisler, Clariá, & Minniti (1997).

Accurate photometry of a sample of very nearby dwarfs obtained by Gonzalez & Piché (Gonzalez & Piché 1992). They also measured $B-V$ colors for these stars. Although the authors did not measure $V-I$ colors, Bessell (1979) has shown that the Stromgren $b-y$ color transforms very well to $V-I$, and we have used his transformation and the very accurate $b-y$ measurements of Eggen (1998) to derive $V-I$ colors for these stars. We have used the six stars in their sample with $B-V \leq 0.51$ to supplement the Landolt standards. Because these stars are so nearby (all have large and accurate parallaxes), reddening corrections are not needed.

It is clear that there is no metallicity dependence in the transformation from $M-T_2$ to $V-I$. It is also possible to transform the $M-T_2$ color to $B-V$, but this is less straightforward because there are different loci for late-type dwarfs and giants in Figure 19. However, for bluer stars such as halo turnoff stars, the relation is single valued, as can be seen in Figure 20. Since there are few metal-poor dwarfs with Washington photometry, we have also plotted the models of Paltoglou & Bell (1994) that are based on synthetic spectra, for dwarfs with solar abundance and $[\text{Fe}/\text{H}] = -2.0$. Paltoglou & Bell (1994) note that their

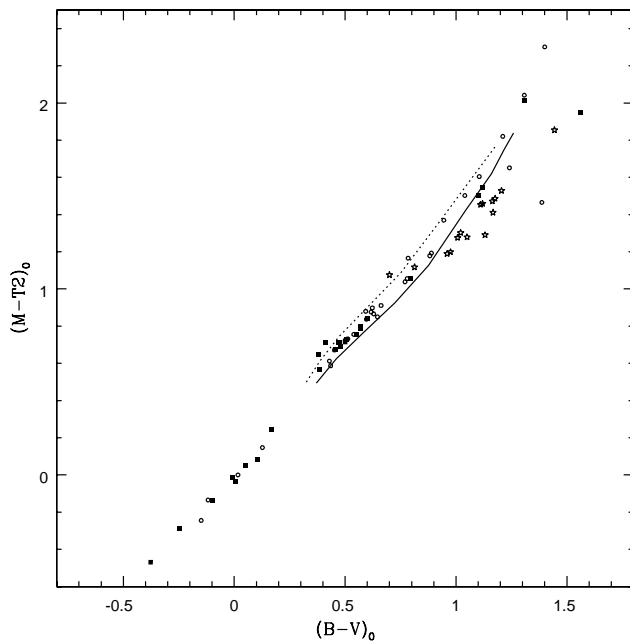


FIG. 20.—Relation between Washington $M-T_2$ and $B-V$ for Landolt-Washington standards (giants plotted as stars, dwarfs as squares, unknown spectral types as circles) and dwarfs from Gonzalez & Piché (1992). The models of Paltoglou & Bell (1994) for solar abundance dwarfs (solid line) and $[\text{Fe}/\text{H}] = -2.0$ dwarfs (dotted line) are also shown.

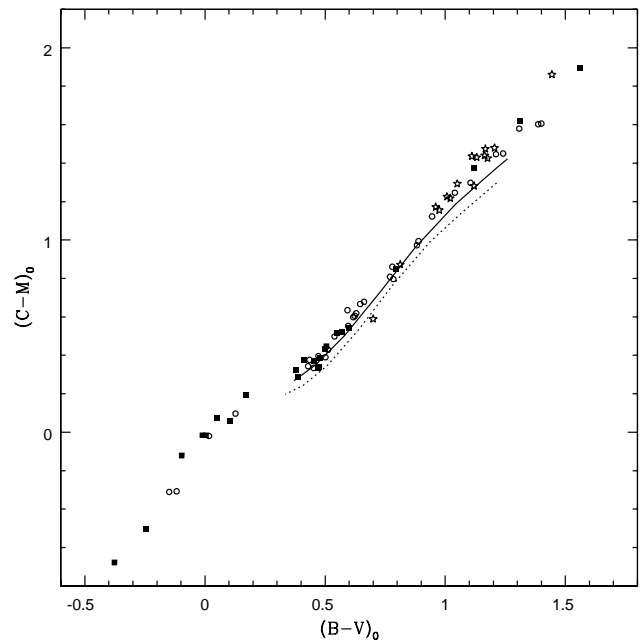


FIG. 21.—Same as Fig. 20, but for the relation between Washington $C-M$ and $B-V$. The models of Paltoglou & Bell (1994) for dwarfs of solar metallicity (solid line) and $[\text{Fe}/\text{H}] = -2.0$ (dotted line) are also shown.

models show good agreement with existing data for temperatures higher than 4500 K ($B-V \simeq 1.0$).

Washington $C-M$ is less useful as a temperature indicator because it has both metallicity sensitivity for late-type stars (from line blanketing around 4000 Å) and some gravity sensitivity for earlier types (from the Balmer jump). We give the relation between $C-M$ and $B-V$ in Figure 21 for completeness.

It is also useful to derive transformations between the Stromgren $b-y$ color and $M-T_2$. This is particularly

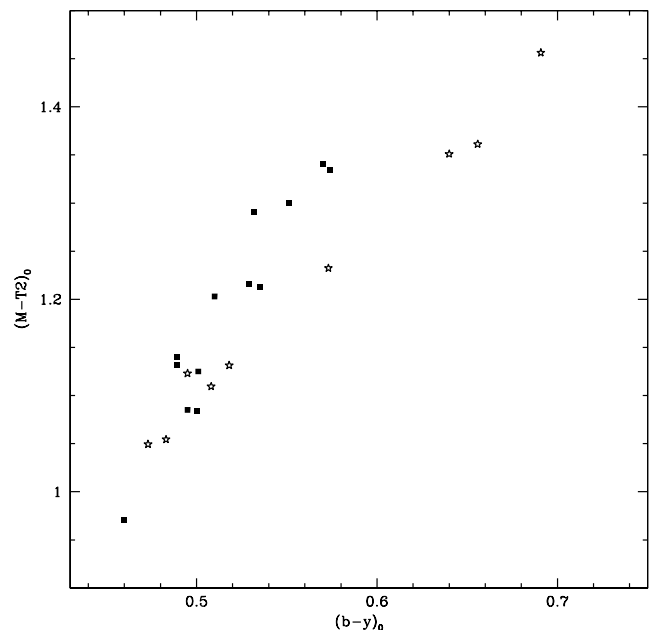


FIG. 22.—Same as Fig. 20, but for the relation between Washington $M-T_2$ and Stromgren $b-y$ for giants and dwarfs.

useful for K star temperatures, because many of our spectroscopic luminosity standards have $b-y$ observations but not $M-T_2$. For main-sequence stars, we used the compilations of Eggen (1998) and Gonzalez & Piché (1992) of photometry of stars from the Yale General Catalog of Trigonometric Parallaxes (van Altena, Lee, & Hoffleit 1991), whose stars have the advantage that they are so close to the Sun that reddening corrections are unlikely to be

needed. For metal-poor giants, we used stars from Bond (1980) with Washington photometry by Geisler (1986). $E(B-V)$ values were taken from Bond (1980) and were smaller than 0.04 in all cases.

Figure 22 shows the relation between these two colors. It can be seen that there are different sequences for red dwarfs and giants, but that the sequences are fairly tight in both cases.

REFERENCES

- Anthony-Twarog, B. J., Twarog, B. A., & Suntzeff, N. B. 1992, *AJ*, 103, 1264
 Armandroff, T. E., & Da Costa, G. S. 1991, *AJ*, 101, 1329
 Bahcall, J. N., & Casertano, S. 1986, *ApJ*, 308, 347
 Bahcall, J. N., & Soniera, R. M. 1984, *ApJS*, 55, 67
 Beers, T. C., Preston, G. W., & Shectman, S. A. 1985, *AJ*, 90, 2089
 Bell, R. A., Paltoglou, G., & Trippico, M. A. 1994, *MNRAS*, 268, 771
 Bessell, M. S. 1979, *PASP*, 91, 589
 ———. 1990, *A&AS*, 83, 357
 Bidelman, W. P., & MacConnell, D. J. 1973, *AJ*, 78, 687
 Bond, H. E. 1980, *ApJS*, 44, 517
 Canterna, R. W. 1976, *AJ*, 81, 228
 Carbon, D. F., Barbuy, B., Kraft, R. P., Friel, E. D., & Suntzeff, N. B. 1987, *PASP*, 99, 335
 Carney, B. W. 1979, *ApJ*, 233, 211
 Carney, B. W., & Latham, D. W. 1987, *AJ*, 93, 116
 Carney, B. W., Latham, D. W., & Laird, J. B. 1989, *AJ*, 97, 423
 Carney, B. W., Latham, D. W., Laird, J. B., & Aguilar, L. A. 1994, *AJ*, 107, 2240
 Ciardullo, R., Jacoby, G. H., & Bond, H. E. 1989, *AJ*, 98, 1648
 Crosswell, K., Latham, D. W., Carney, B. W., Schuster, W., & Aguilar, L. A. 1991, *AJ*, 101, 2078
 Cudworth, K. M. 1979, *AJ*, 84, 1312
 ———. 1985, *AJ*, 90, 65
 Da Costa, G. S., & Armandroff, T. E. 1990, *AJ*, 100, 162
 Davis, M., Efsthathiou, G., Frenk, C. S., White, S. D. M. 1985, *ApJ*, 292, 371
 Dohm-Palmer, R. C., Mateo, M. L., Harding, P., Morris, H. L., Olszewski, E. W., Freeman, K. C., & Norris, J. E. 2000, in preparation
 Eggen, O. J. 1998, *AJ*, 115, 2397
 Eggen, O. J., Lynden-Bell, D., & Sandage, A. R. 1962, *ApJ*, 136, 748
 Fleming, T. A., Liebert, J., & Green, R. F. 1986, *ApJ*, 308, 176
 Flynn, C., & Morrison, H. L. 1990, *AJ*, 100, 1181
 Flynn, C., Sommer-Larsen, J., Christensen, P. R., & Hawkins, M. R. S. 1995, *A&AS*, 109, 171
 Geisler, D. 1984, *PASP*, 96, 723
 ———. 1986, *PASP*, 98, 762
 ———. 1990, *PASP*, 102, 344
 ———. 1996, *AJ*, 111, 480
 Geisler, D., Clariá, J. J., & Minniti, D. 1991, *AJ*, 102, 1836
 ———. 1997, *PASP*, 109, 799
 Geisler, D., Minniti, D., & Clariá, J. J. 1992, *AJ*, 104, 627
 Gonzalez, G., & Piché, F. 1992, *AJ*, 103, 2048
 Governato, F., Moore, B., Cen, R., Stadel, J., Lake, G., & Quinn, T. 1997, *NewA*, 2, 91
 Gunn, J. E. 1995, *BAAS*, 186, 44.05
 Harding, P., Morrison, H. L., Mateo, M. L., Olszewski, E. W., Freeman, K. C., & Norris, J. 2000, in preparation
 Harris, H. C., & Canterna, R. W. 1979, *AJ*, 84, 1750
 Hartwick, F. D. A. 1987, in *The Galaxy*, ed. G. Gilmore & B. Carswell (NATO ASI Ser. C, 207) (Dordrecht: Reidel), 281
 Hauschildt, P. H., Allard, F., & Baron, E. 1999a, *ApJ*, 512, 377
 Hauschildt, P. H., Allard, F., Ferguson, J., Baron, E., & Alexander, D. R. 1999b, *ApJ*, 525, 871
 Hawkins, M. R. S. 1984, *MNRAS*, 206, 433
 Helmi, A., White, S. D. M., de Zeeuw, P. T., & Zhao, H.-S. 1999, *Nature*, 402, 53
 Ibata, R. A., Gilmore, G., & Irwin, M. J. 1994, *Nature*, 370, 194
 Johnson, J. A., & Bolte, M. 1998, *AJ*, 115, 693
 Johnston, K. V., Hernquist, L., & Bolte, M. 1996, *ApJ*, 465, 278
 Johnston, K. V., Spergel, D. V., & Hernquist, L. 1995, *ApJ*, 451, 598
 Kaluzny, J., Wysoka, A., Stanek, K. Z., & Krzeminski, W. 1998, *Acta Astron.*, 48, 439
 Kinman, T. D., Pier, J. R., Suntzeff, N. B., Harmer, D. L., Valdes, F., Hanson, R. B., Klemola, A. R., & Kraft, R. P. 1996, *AJ*, 111, 1164
 Kinman, T. D., Suntzeff, N. B., & Kraft, R. P. 1994, *AJ*, 108, 1722
 Kinman, T. D., Wirtanen, C. A., & Janes, K. A. 1965, *ApJS*, 11, 223
 Klypin, A., Kravtsov, A. V., Valenzuela, O., & Prada, F. 1999, *ApJ*, 522, 82
 Kurucz, R. L. 1992, *Rev. Mexicana Astron. Astrofis.*, 23, 181
 Laird, J. B., Carney, B. W., & Latham, D. W. 1988, *AJ*, 95, 1843
 Landolt, A. 1992, *AJ*, 104, 340
 Lynden-Bell, D. 1999, in *ASP Conf. Ser.* 165, *The Third Stromlo Symposium*, ed. B. K. Gibson, T. S. Axelrod, & M. E. Putnam (San Francisco: ASP), 17
 Lynden-Bell, D., & Lynden-Bell, R. M. 1995, *MNRAS*, 275, 429
 Majewski, S. R. 1992, *ApJS*, 78, 87
 Majewski, S. R., Munn, J. A., & Hawley, S. L. 1994, *ApJ*, 427, L37
 Mateo, M. L. 1998, *ARA&A*, 36, 435
 Méndez, R. A., Platais, I., Girard, T. M., Kozhurina-Platais, V., & van Altena, W. F. 1999, *ApJ*, 524, L39
 Morrison, H. L. 1993, *AJ*, 106, 578
 Morrison, H. L., Flynn, C., & Freeman, K. C. 1990, *AJ*, 100, 1191
 Norris, J. E., & Hawkins, M. R. S. 1991, *ApJ*, 380, 104
 Olszewski, E. W., Harding, P., Mateo, M. L., Morrison, H. L., Freeman, K. C., & Norris, J. 2000, in preparation
 Paltoglou, G., & Bell, R. A. 1994, *MNRAS*, 268, 793
 Pier, J. R. 1982, *AJ*, 87, 1515
 ———. 1983, *ApJS*, 53, 791
 ———. 1984, *ApJ*, 281, 260
 Peterson, R. C. 1981, *ApJ*, 244, 989
 Preston, G. W., Beers, T. C., & Shectman, S. A. 1994, *AJ*, 108, 538
 Preston, G. W., Shectman, S. A., & Beers, T. C. 1991, *ApJ*, 375, 121
 Ratnatunga, K. U., & Freeman, K. C. 1989, *ApJ*, 339, 126
 Reid, N., & Majewski, S. R. 1993, *ApJ*, 409, 635
 Ryan, S. G., & Norris, J. E. 1991, *AJ*, 101, 1835
 Saha, A. 1985, *ApJ*, 289, 310
 Sandage, A., & Fouts, G. 1987, *AJ*, 93, 74
 Sandage, A., & Katem, B. 1964, *ApJ*, 139, 1088
 Sandage, A., Katem, B., & Johnson, H. L. 1977, *AJ*, 82, 389
 Sandage, A., & Luyten, W. J. 1969, *ApJ*, 155, 913
 Sandquist, E. L., Bolte, M., Langer, G. E., Hesser, J. E., & Mendes de Olivera, C. 1999, *ApJ*, 518, 262
 Schlegel, D. J., Finkbeiner, D. P., & Davis, M. 1998, *ApJ*, 500, 525
 Searle, L., & Zinn, R. 1978, *ApJ*, 225, 357
 Seitter, W. C. 1970, *Atlas for Objective Prism Spectra (Bonner Spektral Atlas 1)* (Bonn: Dümmlers)
 Sommer-Larsen, J., & Christensen, P. R. 1985, *MNRAS*, 212, 851
 Suntzeff, N. B., Kinman, T. D., & Kraft, R. P. 1991, *ApJ*, 367, 528
 Totten, E. J., & Irwin, M. J. 1998, *MNRAS*, 294, 1
 Twarog, B. A., & Anthony-Twarog, B. J. 1995, *AJ*, 109, 2828
 Unavane, M., Wyse, R. F. G., & Gilmore, G. 1996, *MNRAS*, 278, 727
 van Altena, W. F., Lee, J. T., & Hoffleit, E. D. 1991, *The General Catalog of Trigonometric Parallaxes* (preliminary version; New Haven: Yale Univ. Obs.)
 Wetterer, C. J., & McGraw, J. T. 1996, *AJ*, 112, 1046
 Zinn, R. J. 1985, *ApJ*, 293, 424
 ———. 1993, in *ASP Conf. Ser.* 48, *The Globular Cluster-Galaxy Connection*, ed. G. H. Smith & J. P. Brodie (San Francisco: ASP), 38